Annals of Biomedical Engineering (© 2006)
DOI: 10.1007/s10439-005-9066-4

Simultaneous Blood–Tissue Exchange of Oxygen, Carbon Dioxide, Bicarbonate, and Hydrogen Ion

RANJAN K. DASH [1,2] and JAMES B. BASSINGTHWAIGHTE [1]

[1]Department of Bioengineering, University of Washington, Seattle, WA 98195 and [2]Present address: Department of Pediatrics, Division of Cardiology, Case Western Reserve University, Cleveland, OH 44106

(Received 19 August 2005; accepted 13 October 2005)

Abstract—A detailed nonlinear four-region (red blood cell, plasma, interstitial fluid, and parenchymal cell) axially distributed convection-diffusion-permeation-reaction-binding computational model is developed to study the simultaneous transport and exchange of oxygen (O_2) and carbon dioxide (CO_2) in the blood–tissue exchange system of the heart. Since the pH variation in blood and tissue influences the transport and exchange of O_2 and CO_2 (Bohr and Haldane effects), and since most CO_2 is transported as HCO_3^- (bicarbonate) via the CO_2 hydration (buffering) reaction, the transport and exchange of HCO_3^- and H^+ are also simulated along with that of O_2 and CO_2. Furthermore, the model accounts for the competitive nonlinear binding of O_2 and CO_2 with the hemoglobin inside the red blood cells (nonlinear O_2–CO_2 interactions, Bohr and Haldane effects), and myoglobin-facilitated transport of O_2 inside the parenchymal cells. The consumption of O_2 through cytochrome-c oxidase reaction inside the parenchymal cells is based on Michaelis–Menten kinetics. The corresponding production of CO_2 is determined by respiratory quotient (RQ), depending on the relative consumption of carbohydrate, protein, and fat. The model gives a physiologically realistic description of O_2 transport and metabolism in the microcirculation of the heart. Furthermore, because model solutions for tracer transients and steady states can be computed highly efficiently, this model may be the preferred vehicle for routine data analysis where repetitive solutions and parameter optimization are required, as is the case in PET imaging for estimating myocardial O_2 consumption.

Keywords—Axially distributed model, Convection-diffusion-permeation-reaction-binding model, Blood–tissue exchange, Oxygen and carbon dioxide transport, Oxygen transport and metabolism, Myoglobin-facilitated oxygen transport, Oxyhemoglobin and carbamino hemoglobin dissociation curves.

INTRODUCTION

The modeling of oxygen transport and metabolism in individual organs is critical for the quantitative understanding of organ and cell functions during physiological responses to change of state, and in pathological states such as ischemia and hypoxia. Oxygen (O_2) transport and metabolism involves convection, diffusion, permeation, chemical reactions, binding and facilitated transport.[20,51,54] Oxygen's binding to hemoglobin (Hb) is affected directly by carbon dioxide (CO_2) levels, pH, temperature, and 2,3-diphosphoglycerate (2,3-DPG) levels, and affected indirectly therefore by bicarbonate (HCO_3^-) buffering, metabolism and tissue acidification, renal acid and base handling, and the hemoglobin mediated nonlinear O_2–CO_2 interactions.[26,37,44,63] A decrease in pH or an increase in CO_2 partial pressure (P_{CO_2}) in the systemic capillaries reduces the affinity of Hb for O_2 (the Bohr effect) and enhances the delivery of O_2 to tissue. A decrease in pH or an increase in O_2 partial pressure (P_{CO_2}) in the pulmonary capillaries reduces the affinity of Hb for CO_2 and enhances the removal of CO_2 from blood into alveoli (Haldane effect). Including the Hb-mediated nonlinear O_2–CO_2 interactions of the Bohr and Haldane effects is critical to the exchange kinetics because of the rapid changes in hemoglobin's affinities to both the gases in the exchange regions.

The interpretation and understanding of alveoli–blood or blood–tissue gas exchange, whether being assessed from the observations of arterial and venous O_2 concentrations,[20,51,54] or by intra-tissue chemical signals such as BOLD MRI[46,53] or hemoglobin and myoglobin spectra,[59,60] or by external detection of tracer content such as ^{15}O-oxygen and ^{15}O-water through PET studies,[27,51,55,62] depends in general on all the factors involved in the dissociation of oxyhemoglobin. To study the dynamics of O_2 transport and metabolism, it is therefore important to account for the transport and exchange of CO_2, HCO_3^-, and H^+ as well as O_2–CO_2 interactions.

The classical Krogh tissue cylinder model,[50] a single cylindrical tissue unit supplied by a single capillary, has been the basis for most of the theoretical studies on microcirculatory oxygen transport to tissue over the past 80 years. Reviews by Hellums *et al.*[37] and Popel[54] and recent studies oriented toward PET ^{15}O-oxygen image analysis by Beyer *et al.*,[20] Deussen and Bassingthwaighte,[27] and

Address correspondence to James B. Bassingthwaighte , PhD, Department of Bioengineering, University of Washington, Harris Hydraulics Building, Room 310, Box 357962, Seattle, WA 98195-7962. Electronic mail: jbb@bioeng.washington.edu

Li *et al*.[51] illustrate the applicability of the geometry that Krogh modeled. Other models based on non-cylindrical geometry have been designed or proposed to reflect the morphological and anatomical structures of the specific tissues.[16–18,31,34,61]

There have been previous studies on simultaneous or dynamic transport and exchange of O_2 and CO_2 in the microcirculation. Hill *et al*.[39–41] and Salathe *et al*.[58] studied the kinetics of O_2 and CO_2 exchange through compartmental modeling by accounting for physical and biochemical processes including the acid–base balance. However, they did not account for convection and diffusion (and hence, concentration gradients) along the capillary length, a major aspect of determining tissue levels and understanding alveolar–arterial oxygen differences. Huang and Hellums[44] developed a quantitative model for convective and diffusive gas (O_2 and CO_2) transport and acid–base regulation in blood flowing in microvessels and in oxygenators while accounting for Bohr and Haldane effects, as discussed in the review by Hellums *et al*.[37] They did not account for the permeation and subsequent consumption of O_2 within the tissue cells, or the production of CO_2. A more complete model of O_2 and CO_2 transport and exchange in the microcirculation is therefore needed for the analysis of experimental data and is the subject of this paper.

To formulate an exchange model, Dash and Bassingthwaighte's[26] equations for oxyhemoglobin and carbamino hemoglobin dissociation curves accounting for pH and Hb-mediated nonlinear O_2–CO_2 interactions were incorporated into a modified three-region blood–tissue exchange model using a highly efficient convection–diffusion algorithm,[13] adding to it the erythrocytes as a convecting fourth region, with velocity higher than that of plasma. The Dash–Bassingthwaighte algorithms for the O_2 and CO_2 saturation curves also provide high computational efficiency since the Hill-type equations are invertible and therefore directly calculable during transients. The simultaneous transport and exchange of O_2, CO_2, HCO_3^-, and H^+ within the blood–tissue exchange system of the heart is analyzed through the use of a nonlinear four-region axially distributed convection-diffusion-permeation-reaction-binding model. Temperature and 2,3-DPG are assumed to be in steady state. The model accounts for the (i) convection in vascular region, axial diffusion in vascular and extra-vascular regions, and permeation through capillary and cell membranes, (ii) CO_2 kinetics and HCO_3^- buffering in blood and tissue, (iii) nonlinear competitive binding of O_2 and CO_2 with Hb, including nonlinear O_2–CO_2 interactions with Hb inside the red blood cells, (iv) myoglobin-facilitated transport of O_2 inside the parenchymal cells, and (v) O_2 consumption and CO_2 production inside the parenchymal cells through cytochrome-c oxidase reaction obeying the Michaelis–Menten kinetics and respiratory quotient.

MATHEMATICAL FORMULATION OF THE MODEL

Blood–Tissue Exchange Unit and Nomenclature

The configuration of the blood–tissue exchange (BTEX) unit for the present study of oxygen (O_2), carbon dioxide (CO_2), bicarbonate (HCO_3^-), and hydrogen ion (H^+) transport and exchange in the heart is similar to the geometry of a classical Krogh cylinder model, e.g., see Li *et al*.[51] as illustrated in Fig. 1. The BTEX unit consists of four concentric regions: The red blood cells (RBC), plasma, interstitial fluid (ISF), and parenchymal cells. Convective flow is F_r (ml g^{-1} min^{-1}), and is one-dimensional, not accounting directly for intravascular velocity profiles. These

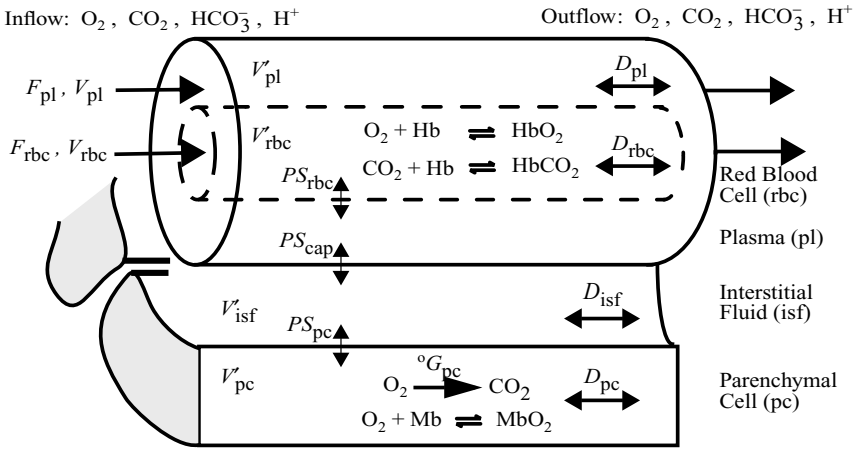

FIGURE 1. Schematic diagram of an axially distributed four-region blood–tissue exchange model for convection, diffusion, permeation, reaction, and binding of O_2, CO_2, HCO_3^-, and H^+ transport and exchange in the heart. Endothelial cells are neglected. For the four species, there are 4 four-region models in parallel. Consumption of O_2 and production of CO_2 occurs only in parenchymal cells, ignoring oxygenases elsewhere. Parameter values are shown in Table 1.

regions are separated by the membranes of RBC, capillary, and parenchymal cells, each of which is characterized by its permeability–surface area product, PS. Because the capillary–tissue exchange length, L, that of the BTEX unit, is almost 1 mm,[6] the model uses partial differential equations[7,9,11] to account for concentration gradients along the length. The anatomical volumes of these regions are denoted by V_{rbc}, V_{pl}, V_{isf}, and V_{pc} (units ml g^{-1}), their fractional water spaces by W_{rbc}, W_{pl}, W_{isf}, and W_{pc} (unitless), and corresponding volumes of distribution by V'_{rbc}, V'_{pl}, V'_{isf}, and V'_{pc} (units ml g^{-1}), which are the anatomical volumes times their fractional water spaces, e.g. $V'_{isf} = V_{isf} \times W_{isf}$.

The radial diffusion (perpendicular to the capillary length) of a species (O_2, CO_2, HCO_3^-, or H^+) within a region (RBC, plasma, ISF, or parenchymal cells) is treated as if instantaneous because the radial diffusion distances are only a few microns (maximum of about 8 microns for half intercapillary distances in the heart) and the relaxation times for radial gradients are very short, a few milliseconds, compared to the average capillary transit times of a second or so.[9] This assumption is further justified, for the heart, by there usually being four capillaries around each myocyte. Additional evidence was found in experiments by Deussen and Bassingthwaighte[27] in which oxygen was observed to be flow-limited in its exchange with tissue when oxygen consumption was blocked by cyanide in RBC-perfused rabbit hearts, thus illustrating that neither the set of membranes from RBC to mitochondria nor radial diffusion caused any hindrance to exchange (not reported in the Deussen and Bassingthwaighte,[27] paper). Given the rapid dissipation of intracapillary radial concentration gradients, the RBC can be well represented as a central column of fluid surrounded by plasma, a situation mathematically similar to Hb being dispersed throughout the plasma.[20,51] (This assumption fails at low hematocrits, Hct, as shown by Hellums[36]). The RBC and plasma move by plug flow with different velocities; RBC move faster than the plasma, being in the higher velocity central stream. Plasma has zero velocity at the capillary wall, but because the radial diffusion is so fast the velocity profile is considered uniform at the mean velocity of the fluid. This contrasts with *arterial* velocity profiles because the peak velocity is about 1.6 times the average velocity.[5] The small vessel (capillary) hematocrits average perhaps three-fourth of large vessel hematocrits, a Fahraeus–Lindquist effect[32] with RBC velocities being 30–50% higher than plasma velocities. The blood flow (F_{bl}) in the capillary is assumed to be steady, so the RBC and plasma flows (F_{rbc} and F_{pl}) can be considered as constants. F_{bl}, F_{rbc}, and F_{pl} are in units of ml min^{-1} (g of tissue)$^{-1}$.

In the blood space (RBC and plasma), there is both convection and diffusion (axial dispersion). The axial dispersion within a region is characterized by a pseudo diffusion or dispersion coefficient D (units cm^2 s^{-1}). D_{pl} characterizes the overall axial dispersion in the plasma by the combined processes of molecular diffusion, axial velocity distribution, flow disturbances, eddy currents, and mixing accompanying RBC rotation. Thus, the value of D_{pl} is much higher than the coefficient of molecular diffusion in the plasma. It is about 1×10^{-4} cm^2 s^{-1} for O_2.[51] We consider it to be approximately the same for CO_2, HCO_3^-, and H^+. D_{rbc} characterizes the overall axial dispersion of RBC (as RBC are suspended particles in the plasma) via all the above processes, except that axial molecular diffusion of Hb is negligible. Thus, D_{rbc} is about 5 to 10×10^{-5} cm^2 s^{-1}.[51] The dispersion coefficient of a solute species within RBC is considered to have the same dispersion coefficient as RBC. The axial transport (along the capillary length, L) of a species in the extra-vascular region (ISF and parenchymal cells) is due to axial molecular diffusion dissipating any concentration gradients, and its effect on the shapes of concentration–time curves is augmented by irregularity in the alignments of the capillaries in sets of neighboring BTEX units.

Offset positioning of starting and ending points of neighboring capillaries results not only in heterogeneity of axial diffusion distances, reducing the effective lengths and reducing the axial concentration gradients,[16,17] but also allows tracer solutes to take a short path from near the entrance of one capillary to the exit region of another, having quantitatively the same effect as enhanced extra-vascular axial diffusion. Accordingly, tracer water dilution curves show a small amount of diffusional shunting from inflow to outflow.[8] To account for the heterogeneity in D/L, values of D_{isf} and D_{pc} are higher than the normal intra-myocardial diffusion coefficients.[56,64] Following the method of Safford *et al*.[57] for serial/parallel diffusion through and around cells and accounting for the heterogeneity in D/L, we set the values for dispersion coefficients D_{isf} and D_{pc} for all small solutes to 1×10^{-4} cm^2 s^{-1}.[27,51] The dispersion smooths axial gradients in each region but does not influence estimation of O_2 consumption rates.

The transmembrane transport (permeation) of a species across the membranes is assumed to be passive and is characterized by the permeability surface area product parameters PS (units ml min^{-1} g^{-1}), i.e., the product of barrier permeability, P (cm min^{-1}), and surface area, S (cm^2 g^{-1}). The PS is the barrier conductance for the solute: Permeability P is a diffusion coefficient in the barrier material D_m divided by the barrier thickness d_m (i.e., $P = D_m/d_m$). Solute species dissolving in the phospholipid bilayer have high Ps. The permeation of HCO_3^- occurs through the band-3 anion transporter and that of H^+ through the proton channels, thus their PSs are about an order of magnitude lower than those for dissolved gases such as O_2 and CO_2 (see Table 1 for values), and yet are still so high that the barrier has almost no influence on the kinetics of tracer transport. (However, the transport of CO_2 is slowed when carbonic anhydrase is inhibited, not because of a change in membrane PS, but

TABLE 1. Representative values of parameters used in model simulation (for more description on a particular parameter, see the appropriate running text).

Symbol	Definition	Value	Unit	Ref.
α_{O_2}	Solubility of O_2 in water at body temperature	1.46×10^{-6}	M mmHg^{-1} P_{O_2})	35
α_{CO_2}	Solubility of CO_2 in water at body temperature	3.27×10^{-5}	M mmHg^{-1} P_{CO_2})	2
β_{rbc}	Buffering capacity in RBC	54×10^{-3}	M pH^{-1} unit	41,58
β_{pl}	Buffering capacity in plasma	6×10^{-3}	M pH^{-1} unit	41,58
β_{isf}	Buffering capacity in ISF	24×10^{-3}	M pH^{-1} unit	*
β_{pc}	Buffering capacity in PC	45×10^{-3}	M pH^{-1} unit	*
C_{Hbrbc}	Concentration of Hb in the water space of RBC	7.2×10^{-3}	M	27, 51,*
C_{Mbpc}	Concentration of Mb in the water space of PC	0.5×10^{-3}	M	27,51
${}^{s}D_{r}$	Dispersion coefficient of species 's' in region 'r'	1×10^{-4}	cm^2 s^{-1}	17, 27, 51,*
F_{bl}	Flow of blood	1	ml min^{-1} g^{-1}	9,27,51
F_{rbc}	Flow of RBC (Hct $\times$ F_{bl})	0.45	ml min^{-1} g^{-1}	51,*
F_{pl}	Flow of plasma ($F_{bl} - F_{rbc}$)	0.55	ml min^{-1} g^{-1}	51,*
Hct	Large-vessel hematocrit	0.45	ml ml^{-1}	51
Hct_{cap}	Capillary hematocrit [see Eq. (14d)]	0.34	ml ml^{-1}	51,*
kf_1	Modified rate constant in forward direction of CO_2 hydration reaction ($kf_1 = [H_2O]kf'_1$)	0.12	s^{-1}	39, 40, 41,*
kb_1	Modified rate constant in backward direction of CO_2 hydration reaction ($kb_1 = kb'_1/K''_1$)	162,000	M^{-1} s^{-1}	39, 40, 41,*
K''_1	Ionization constant for H_2CO_3	5.5×10^{-4}	M	39,40,41
K'_1	Equilibrium constant for hydration of CO_2 ($K'_1 = [H_2O]kf'_1/kb'_1$)	1.35×10^{-3}	Unitless	*
K_1	Equilibrium constant for the overall CO_2 hydration reaction ($K_1 = kf_1/kb_1 = K'_1K''_1$)	7.43×10^{-7}	M	39, 40, 41,*
K''_2	Ionization constant for HmNHCOOH	1×10^{-6}	M	1,41
K'_2	Equilibrium constant for uptake of CO_2 by reduced hemoglobin ($K'_2 = kf'_2/kb'_2 = K_2/K''_2$)	29.5	M^{-1}	*
K_2	Equilibrium constant for the overall uptake of CO_2 by reduced hemoglobin ($K_2 = K'_2K''_2$)	2.95×10^{-5}	Unitless	1,41
K''_3	Ionization constant for O_2HmNHCOOH	1×10^{-6}	M	1,41
K'_3	Equilibrium constant for uptake of CO_2 by oxygenated hemoglobin ($K'_3 = kf'_3/kb'_3 = K_3/K''_3$)	25.1	M^{-1}	*
K_3	Equilibrium constant for the overall uptake of CO_2 by oxygenated hemoglobin ($K_3 = K'_3K''_3$)	2.51×10^{-5}	Unitless	1,41
K''_4	Proportionality equilibrium constant for uptake of O_2 by hemoglobin [see Eq. (6)]	202123	M^{-1}	
K''_5	Ionization constant for $HmNH_3^+$	2.63×10^{-8}	M	1
K''_6	Ionization constant for $O_2HmNH_3^+$	1.91×10^{-8}	M	1
K_m	Michaelis–Menten constant for cytochromic-c oxidation in PC	7×10^{-7}	M	17,31
K_{rbc}	Catalytic factor in CO_2 hydration reaction in RBC	13,000	Unitless	39, 40, 41
K_{pl}	Catalytic factor in CO_2 hydration reaction in plasma	100	Unitless	*
K_{isf}	Catalytic factor in CO_2 hydration reaction in ISF	5000	Unitless	*
K_{pc}	Catalytic factor in CO_2 hydration reaction in PC	10,000	Unitless	*
L	Length of the capillary	1	mm	6,9,27,51
n_0	Exponent on $[O_2]/[O_2]_S$ in expression for K'_4	1.7	Unitless	
n_1	Exponent on $[H^+]_S/[H^+]$ in expression for K'_4	1.06	Unitless	
n_2	Exponent on $[CO_2]_S/[CO_2]$ in expression for K'_4	0.12	Unitless	
$P_{O_{2,art}}$	Standard O_2 partial pressure in the arterial end	100	mmHg	51, 58
$P_{CO_{2,art}}$	Standard CO_2 partial pressure in the arterial end	40	mmHg	58
$pH_{pl,art}$	Standard pH level in plasma in the arterial end ($pH_{pl,art} = -\log[H^+]_{pl,art}$)	7.4	Unitless	41,58
$pH_{rbc,art}$	Standard pH level in RBC in the arterial end ($pH_{rbc,art} = -\log[H^+]_{rbc,art}$)	7.24	Unitless	41,58
P_{50}^{Hb}	Level of P_{O_2} at which Hb is 50% saturated by O_2	26.8	mmHg	22, 45, 66
P_{50}^{Mb}	Level of P_{O_2} at which Mb is 50% saturated by O_2	2.39	mmHg	17,59,60
${}^{(o,c)}PS_{bc}$	Permeability surface area product of the RBC membrane for O_2 and CO_2	1000	ml min^{-1} g^{-1}	51
${}^{(o,c)}PS_{cap}$	Permeability surface area product of the capillary membrane for O_2 and CO_2	200	ml min^{-1} g^{-1}	51

TABLE 1. Continued.

Symbol	Definition	Value	Unit	Ref.
${}^{(o,c)}PS_{pc}$	Permeability surface area product of the PC membrane for O_2 and CO_2	2000	ml min^{-1} g^{-1}	51
${}^{(b,h)}PS_{rbc}$	Permeability surface area product of the RBC membrane for HCO_3^- and H^+	100	ml min^{-1} g^{-1}	*
${}^{(b,h)}PS_{cap}$	Permeability surface area product of the capillary membrane for HCO_3^- and H^+	20	ml min^{-1} g^{-1}	*
${}^{(b,h)}PS_{pc}$	Permeability surface area product of the PC membrane for HCO_3^- and H^+	200	ml min^{-1} g^{-1}	*
RQ	Respiratory quotient (rate CO_2 production divided by rate O_2 consumption)	0.8	Unitless	44,58
R_{rbc}	Gibbs–Donnan ratio across the RBC membrane	0.69	Unitless	41,58,66
R_{cap}	Gibbs–Donnan ratio across the capillary membrane	0.63	Unitless	*
R_{pc}	Gibbs–Donnan ratio across the PC membrane	0.79	Unitless	*
R_{vel}	Ratio of RBC to plasma velocity	1.6	Unitless	6,32,51
V_{max}	Maximum rate of cytochromic oxidation in PC	2.5×10^{-6}	mol min^{-1} g^{-1}	17,51
V_{cap}	Anatomical volume of capillary	0.07	ml g^{-1}	6,9,27,51
V_{rbc}	Anatomical volume of RBC ($Hct_{cap} \times V_{cap}$)	0.024	ml g^{-1}	51,*
V_{pl}	Anatomical volume of plasma ($V_{cap} - V_{rbc}$)	0.046	ml g^{-1}	51,*
V_{isf}	Anatomical volume of ISF	0.2	ml g^{-1}	27,51
V_{pc}	Anatomical volume of PC	0.7	ml g^{-1}	27,51
V_r'	Volume of distribution (water space) in a region 'r'	$V_r \times W_r$	ml g^{-1}	51,*
W_{rbc}	Fractional water space of RBC	0.72	ml ml^{-1}	51,*
W_{pl}	Fractional water space of plasma	0.94	ml ml^{-1}	51
W_{isf}	Fractional water space of ISF	0.92	ml ml^{-1}	51,*
W_{pc}	Fractional water space of PC	0.8	ml ml^{-1}	51

Note. Left superscripts denote substrate, s; oxygen, o; carbon dioxide, c; hydrogen ion, h; and bicarbonate, b.
*Calculated or correlated from the data in the literature.

because of slow transformation from bicarbonate to CO_2, the form in which most of the flux occurs.)

The consumption of O_2 and production of CO_2 occurs only in parenchymal cells, ignoring oxygenases elsewhere, and is characterized by the "gulosity" parameter ${}^{\circ}G_{pc}$ (units ml min^{-1} g^{-1}); ${}^{\circ}G_{pc}$ is dependent on intracellular oxygen concentration, assuming Michaelis–Menten kinetics, which is effectively zero-order when P_{O_2} is high compared to its K_m (which is the case usually) and first-order when O_2 concentration is low. The CO_2 is produced inside the parenchymal cells from oxidative metabolism of glucose, proteins, and fatty acids. The ratio of the rate of CO_2 production to the rate of O_2 consumption is the respiratory quotient RQ: it is 1.0 for glucose metabolism, 0.8 for protein metabolism, and 0.7 for fat metabolism. In myocardium, RQ is normally around 0.8, indicating more fat usage than glucose.

The formation of HCO_3^- is governed by the CO_2 hydration reaction which, in aqueous solution, is slow. However, in RBC, ISF, and parenchymal cells this reaction is facilitated by the enzyme carbonic anhydrase in cytosol and on the membranes. The membranes of RBC, capillary, and parenchymal cells are fairly permeable to HCO_3^- (through the band-3 transporter), allowing dissipation of gradients. Charge neutrality is attained by the diffusion of chloride ions (Cl^-) from a region of higher negative charge to a region of higher positive charge (the chloride shift) until the Gibbs–Donnan electrochemical equilibrium conditions are reached[39–41,58]:

$$R_{rbc} = \frac{[HCO_3^-]_{rbc}}{[HCO_3^-]_{pl}} = \frac{[Cl^-]_{rbc}}{[Cl^-]_{pl}} = \frac{[H^+]_{pl}}{[H^+]_{rbc}}, \quad (1a)$$

$$R_{cap} = \frac{[HCO_3^-]_{isf}}{[HCO_3^-]_{pl}} = \frac{[Cl^-]_{isf}}{[Cl^-]_{pl}} = \frac{[H^+]_{pl}}{[H^+]_{isf}}, \quad (1b)$$

$$R_{pc} = \frac{[HCO_3^-]_{pc}}{[HCO_3^-]_{isf}} = \frac{[Cl^-]_{pc}}{[Cl^-]_{isf}} = \frac{[H^+]_{isf}}{[H^+]_{pc}}, \quad (1c)$$

where R_{rbc}, R_{cap}, and R_{pc} (unitless) are the Gibbs–Donnan ratios across the membranes of RBC, capillary, and parenchymal cells. Under standard physiological conditions, pH in plasma, RBC, ISF, and parenchymal cells is about 7.4, 7.24, 7.2, and 7.1, respectively. Thus, $R_{rbc} = 0.69$, $R_{cap} = 0.63$, and $R_{pc} = 0.79$. The transport of Cl^- is not calculated in the model, but its regional equilibrium concentrations can be calculated from these equations.

Dynamic Mass Balance Equations for O_2, CO_2, HCO_3^-, *and* H^+

The governing equations for each of the four species (O_2, CO_2, HCO_3^-, and H^+) in each of the four regions (RBC, plasma, ISF, and parenchymal cells) of the BTEX

unit are formulated by considering the detailed biophysical and biochemical phenomena discussed above with the constraint of mass conservation. The molar concentrations $C(x, t)$, are functions of time (t) and axial distance (x) along the capillary of length (L, cm).

The nomenclature is based on that approved by the American Physiological Society[10]: ${}^{s}C_{r}$ and ${}^{s}D_{r}$ denote the concentration and axial dispersion coefficient of a species "s" in a region "r"; ${}^{s}PS_{m}$ denotes the permeability surface area product for a species, s, across a membrane, m; s is one of the species O_2, CO_2, HCO_3^-, and H^+ (pre-superscripted as o, c, b, and h), r is one of the regions RBC, plasma, ISF, and parenchymal cells (subscripted as rbc, pl, isf, and pc), and m is one of the membranes RBC, capillary, and parenchymal cells (subscripted as rbc, cap, and pc). Table 1 lists parameters, representative values, and units.

Equations for Oxygen

Oxygen is transported in the plasma and ISF only in a dissolved form. However, in RBC and parenchymal cells it is transported in the dissolved form as well as in combination with Hb and myoglobin (Mb) as oxyhemoglobin (HbO_2) and oxymyoglobin (MbO_2). The dissolved O_2 in RBC and parenchymal cells is assumed to be in constant equilibrium with the HbO_2 and MbO_2 assuming that the kinetics of O_2 binding to Hb and Mb are fast compared with those of the transport processes. See Dash and Bassingthwaighte[26] for detailed reaction schema and kinetic parameters. The equations which follow use the equilibrium constants for the binding. The regional transport equations for convection, diffusion, permeation, and reaction are

$$\frac{\partial({}^{\circ}C_{rbc} + C_{HbO_2})}{\partial t} = -\frac{F_{rbc}L}{V_{rbc}}\frac{\partial({}^{\circ}C_{rbc} + C_{HbO_2})}{\partial x} - \frac{{}^{\circ}PS_{rbc}}{V'_{rbc}}({}^{\circ}C_{rbc} - {}^{\circ}C_{pl}) + {}^{\circ}D_{rbc}\frac{\partial^2({}^{\circ}C_{rbc} + C_{HbO_2})}{\partial x^2}, \quad (2a)$$

$$\frac{\partial {}^{\circ}C_{pl}}{\partial t} = -\frac{F_{pl}L}{V_{pl}}\frac{\partial {}^{\circ}C_{pl}}{\partial x} + \frac{{}^{\circ}PS_{rbc}}{V'_{pl}}({}^{\circ}C_{rbc} - {}^{\circ}C_{pl}) - \frac{{}^{\circ}PS_{cap}}{V'_{pl}}({}^{\circ}C_{pl} - {}^{\circ}C_{isf}) + {}^{\circ}D_{pl}\frac{\partial^2 {}^{\circ}C_{pl}}{\partial x^2}, \quad (2b)$$

$$\frac{\partial {}^{\circ}C_{isf}}{\partial t} = \frac{{}^{\circ}PS_{cap}}{V'_{isf}}({}^{\circ}C_{pl} - {}^{\circ}C_{isf}) - \frac{{}^{\circ}PS_{pc}}{V'_{isf}}({}^{\circ}C_{isf} - {}^{\circ}C_{pc}) + {}^{\circ}D_{isf}\frac{\partial^2 {}^{\circ}C_{isf}}{\partial x^2}, \quad (2c)$$

$$\frac{\partial({}^{\circ}C_{pc} + C_{MbO_2})}{\partial t} = \frac{{}^{\circ}PS_{pc}}{V'_{pc}}({}^{\circ}C_{isf} - {}^{\circ}C_{pc}) - \frac{{}^{\circ}G_{pc}}{V'_{pc}}{}^{\circ}C_{pc} + {}^{\circ}D_{pc}\frac{\partial^2({}^{\circ}C_{pc} + C_{MbO_2})}{\partial x^2}, \quad (2d)$$

where C_{HbO_2} and C_{MbO_2} are the concentrations of hemoglobin- and myoglobin-bound O_2 in RBC and parenchymal cells. The concentration of dissolved O_2 in a region r, ${}^{\circ}C_r$, is related to the partial pressure of O_2 in that region, $P_{O_{2,r}}$, by Henry's law: ${}^{\circ}C_r = \alpha_{O_2} \times P_{O_{2,r}}$, where α_{O_2} is the solubility of O_2 in water.

Equations for C_{HbO_2} and C_{MbO_2}

One mole of Hb can bind with four moles of O_2 and one mole of Mb can bind with one mole of O_2, so the concentrations of Hb- and Mb-bound O_2(C_{HbO_2} and C_{MbO_2}) can be calculated from the O_2 saturations of Hb and Mb (S_{HbO_2} and S_{MbO_2}) using

$$C_{HbO_2} = 4C_{Hbrbc}S_{HbO_2} \quad \text{and} \quad C_{MbO_2} = C_{Mbpc}S_{MbO_2}, \quad (3)$$

where C_{Hbrbc} and C_{Mbpc} are the concentrations of Hb and Mb in the water spaces of RBC and parenchymal cells. With an Hb content of 0.333 g ml^{-1} RBC (0.15 g ml^{-1} blood, Hct = 0.45), an RBC water fraction of 0.72 ml ml^{-1} RBC, and $MW_{Hb} = 64,458$ for the tetramer, then $C_{Hbrbc} = 7.2$ mM. Myoglobin concentrations in myocardial cell vary widely among species, but this example model used those in rabbit hearts, an Mb content of 0.0067 g ml^{-1} cell (0.005 g ml^{-1} tissue and cell volume fraction in tissue of 0.75 ml ml^{-1} tissue), a myocyte water fraction of 0.8 ml ml^{-1} cell, and $MW_{Mb} = 16,800$, gives $C_{Mbpc} = 0.5$ mM.

Equations for S_{HbO_2} and S_{MbO_2}

Of the several mathematical formulas available for describing the relationship of P_{O_2} to the O_2 saturation of Hb and Mb, S_{HbO_2} and S_{MbO_2} (see Popel[54] for a review), the modified Hill equation for S_{HbO_2} of Dash and Bassingthwaighte[26] allows the effects of intra-RBC pH, P_{CO_2}, 2,3-DPG and temperature as well as the nonlinear O_2–CO_2 interactions to be incorporated into the model for simultaneous O_2 and CO_2 transport and exchange during transients. The expressions for S_{HbO_2} and S_{MbO_2} are

$$S_{HbO_2} = \frac{K_{HbO_2}{}^{\circ}C_{rbc}}{1 + K_{HbO_2}{}^{\circ}C_{rbc}} \quad \text{and} \quad S_{MbO_2} = \frac{K_{MbO_2}{}^{\circ}C_{pc}}{1 + K_{MbO_2}{}^{\circ}C_{pc}}, \quad (4)$$

where K_{HbO_2} (with units M^{-1}) is a function of P_{O_2}, P_{CO_2}, and pH, or equivalently ${}^{\circ}C_{rbc}$, ${}^{c}C_{rbc}$, and ${}^{h}C_{rbc}$, and K_{MbO_2}

(M^{-1}) are given by

$$K_{HbO_2} = \frac{K_4'\left(K_3'\,{}^{c}C_{rbc}\left\{1+\frac{K_3''}{{}^{h}C_{rbc}}\right\}+\left\{1+\frac{{}^{h}C_{rbc}}{K_6''}\right\}\right)}{\left(K_2'\,{}^{c}C_{rbc}\left\{1+\frac{K_2''}{{}^{h}C_{rbc}}\right\}+\left\{1+\frac{{}^{h}C_{rbc}}{K_5''}\right\}\right)}$$

$$\text{and}\quad K_{MbO_2} = \frac{1}{\alpha_{O_2} P_{50}^{Mb}}, \tag{5}$$

and K_4' (with units M^{-1}) is given by

$$K_4' = K_4''\left\{\frac{{}^{\circ}C_{rbc}}{{}^{\circ}C_{rbc,S}}\right\}^{n_0}\left\{\frac{{}^{h}C_{rbc}}{{}^{h}C_{rbc,S}}\right\}^{-n_1}\left\{\frac{{}^{c}C_{rbc}}{{}^{c}C_{rbc,S}}\right\}^{-n_2}. \tag{6}$$

The equilibrium constants K_2', K_2'', K_3', K_3'', K_4'', K_5'', and K_6'' and the empirical exponents n_0, n_1, and n_2 are as defined in Dash and Bassingthwaighte[26] (see Table 1 for values). The subscript S refers to values in standard physiological conditions at 37°C. The concentration of 2,3-DPG is assumed fixed at 4.65 mM. P_{50}^{Mb} is the value of P_{O_2} at which Mb is 50% saturated by O_2; $P_{50}^{Mb} = 2.39$ mmHg[59,60]; the P_{50}^{Hb} for human hemoglobin is about 26.8 mmHg.

Michaelis–Menten Kinetics for Oxygen Consumption

The consumption of oxygen is facilitated by the mitochondrial cytochrome-c oxidase reaction and regulated via the availability of substrates (ADP, Pi, NADH, and FADH) to mitochondrial electron transport chain. The oxygen consumption in Eq. (2d) is the product of a "gulosity" ${}^{\circ}G_{pc}$ (with units of a clearance or flow) times the concentration, with ${}^{\circ}G_{pc}$ for MM kinetics being

$${}^{\circ}G_{pc} = \frac{V_{max}}{K_m + {}^{\circ}C_{pc}}, \tag{7}$$

where V_{max} (mol min^{-1} g^{-1}) is the maximal rate of O_2 consumption and K_m is the Michaelis constant. Under standard physiological conditions, V_{max} is about 2.5×10^{-6} mol min^{-1} g^{-1} and K_m about 7×10^{-7} M (which corresponds to about 0.5 mmHg in the units of partial pressure as $\alpha_{O_2} = 1.46 \times 10^{-6}$ M $mmHg^{-1}$.[17,31,51] The estimate of K_m about 0.7 μM is a functional one that makes excellent sense relative to myoglobin P_{50}^{Mb} about 2.39 mmHg. Furthermore, the K_m value from *in vitro* measurements on isolated mitochondria are generally found to be 0.5–1 Torr Po_2, about 0.7 μM [O_2]. A K_m value of 0.7 μM is also in agreement with the "apparent" K_m value of 0.8 μM estimated by Korzeniewski and Zoladz[49] for the cytochrome-c oxidase reaction.

Equations for Carbon Dioxide

CO_2 along with other metabolic by-products such as water (H_2O) has a positive net flux from tissue to effluent blood. It undergoes reactions during its transport and exchange process.[26,37] In all regions, CO_2 is transported in both dissolved form and as bicarbonate ions, HCO_3^-. In RBC, it is also in combination with hemoglobin as carbamino hemoglobin, $HbCO_2$, which is assumed to be in constant equilibrium with the dissolved CO_2. The partial differential equations for CO_2 in the four regions are

$$\begin{aligned}\frac{\partial({}^{c}C_{rbc}+C_{HbCO_2})}{\partial t} = &-\frac{F_{rbc}L}{V_{rbc}}\frac{\partial({}^{c}C_{rbc}+C_{HbCO_2})}{\partial x}\\ &-\frac{{}^{c}PS_{rbc}}{V_{rbc}'}({}^{c}C_{rbc}-{}^{c}C_{pl})\\ &+{}^{c}D_{rbc}\frac{\partial^2({}^{c}C_{rbc}+C_{HbCO_2})}{\partial x^2}\\ &+K_{rbc}(kb_1\,{}^{b}C_{rbc}\,{}^{h}C_{rbc}\\ &-kf_1\,{}^{c}C_{rbc})\end{aligned} \tag{8a}$$

$$\begin{aligned}\frac{\partial {}^{c}C_{pl}}{\partial t} = &-\frac{F_{pl}L}{V_{pl}}\frac{\partial {}^{c}C_{pl}}{\partial x}+\frac{{}^{c}PS_{rbc}}{V_{pl}'}({}^{c}C_{rbc}-{}^{c}C_{pl})\\ &-\frac{{}^{c}PS_{cap}}{V_{pl}'}({}^{c}C_{pl}-{}^{c}C_{isf})\\ &+{}^{c}D_{pl}\frac{\partial^{2c}C_{pl}}{\partial x^2}+K_{pl}(kb_1\,{}^{b}C_{pl}\,{}^{h}C_{pl}\\ &-kf_1\,{}^{c}C_{pl}),\end{aligned} \tag{8b}$$

$$\begin{aligned}\frac{\partial {}^{c}C_{isf}}{\partial t} = &\frac{{}^{c}PS_{cap}}{V_{isf}'}({}^{c}C_{pl}-{}^{c}C_{isf})\\ &-\frac{{}^{c}PS_{pc}}{V_{isf}'}({}^{c}C_{isf}-{}^{c}C_{pc})\\ &+{}^{c}D_{isf}\frac{\partial^2\,{}^{c}C_{isf}}{\partial x^2}\\ &+K_{isf}(kb_1\,{}^{b}C_{isf}\,{}^{h}C_{isf}-kf_1\,{}^{c}C_{isf}),\end{aligned} \tag{8c}$$

$$\begin{aligned}\frac{\partial {}^{c}C_{pc}}{\partial t} = &\frac{{}^{c}PS_{pc}}{V_{pc}'}({}^{c}C_{isf}-{}^{c}C_{pc})\\ &+{}^{c}D_{pc}+\frac{\partial^2\,{}^{c}C_{pc}}{\partial x^2}\\ &+RQ\frac{{}^{o}G_{pc}}{V_{pc}'}\,{}^{o}C_{pc}\\ &+K_{pc}(kb_1\,{}^{b}C_{pc}\,{}^{h}C_{pc}-kf_1\,{}^{c}C_{pc}),\end{aligned} \tag{8d}$$

where K_{rbc}, K_{pl}, K_{isf}, and K_{pc} (unitless) are the catalytic factors for CO_2 hydration reaction due to the presence of enzyme carbonic anhydrase in the four regions of the BTEX unit; K_{pl} is small, perhaps less than 100, but K_{rbc}, K_{isf}, and K_{pc} are of the order of 10,000; also $kf_1 = [H_2O]kf_1' = 0.12$ s^{-1} and $kb_1 = kb_1'/K_1'' = 89$ $s^{-1}/5.5 \times 10^{-4}$ M = 162,000 M^{-1} s^{-1}. These parameters are obtained from Hill

et al.,[39–41] Salathe *et al.*,[58] and Huang and Hellums.[44] The last term in each of the equations represents the net rate of transformation of CO_2 to or from bicarbonate. In Eq. (8d), the rate of production of CO_2 inside the parenchymal cells is expressed as the rate of consumption of O_2 times the respiratory quotient, RQ. The concentration of dissolved CO_2 in a region r, ${}^{c}C_r$, is related to the partial pressure of CO_2 in that region, $P_{CO_{2,r}}$, by Henry's law: ${}^{c}C_r = \alpha_{CO_2} \times P_{CO_{2,r}}$, where α_{CO_2} is the solubility of CO_2 in water. At body temperature ($T = 37^{\circ}$C), $\alpha_{CO_2} = 3.27 \times 10^{-5}$ M mmHg^{-1}.[2]

Equations for C_{HbCO_2} and S_{HbCO_2}

As one mole of Hb binds with 4 moles of CO_2, the concentration of Hb-bound CO_2 (C_{HbCO_2}) can be calculated from CO_2 saturation of hemoglobin (S_{HbCO_2}) using the formula:

$$C_{HbCO_2} = 4C_{Hbrbc} S_{HbCO_2}. \tag{9}$$

In present notations, the equation for S_{HbCO_2} from[26] is given by

$$S_{HbCO_2} = \frac{K_{HbCO_2}\,{}^{c}C_{rbc}}{1 + K_{HbCO_2}\,{}^{c}C_{rbc}}, \tag{10}$$

where K_{HbCO_2} (a function of P_{O_2}, P_{CO_2}, and pH, or ${}^{\circ}C_{rbc}$, ${}^{c}C_{rbc}$, and ${}^{h}C_{rbc}$) is given by

$$K_{HbCO_2} = \frac{\left(K_2'\left\{1 + \frac{K_2''}{{}^{h}C_{rbc}}\right\} + K_3'K_4'\left\{1 + \frac{K_3''}{{}^{h}C_{rbc}}\right\}{}^{\circ}C_{rbc}\right)}{\left(\left\{1 + \frac{{}^{h}C_{rbc}}{K_5''}\right\} + K_4'\left\{1 + \frac{{}^{h}C_{rbc}}{K_6''}\right\}{}^{\circ}C_{rbc}\right)}. \tag{11}$$

Thus, Eq. (10) for carbon dioxide and Eq. (4) for oxygen can both be calculated directly from the ambient concentrations of the free unbound solutes at each instant in time, critical to obtaining rapid computation. Equation (6) defines K_4'.

Equations for Bicarbonate Ions

The amount of CO_2 transported as bicarbonate ions (HCO_3^-) is governed by the CO_2 hydration reaction. At equilibrium or steady state, the exchange of HCO_3^- through the band-3 anion channel is governed by the Gibbs–Donnan electrochemical equilibrium conditions: Eqs. (1a)–(1c). The dynamics of transport and exchange of HCO_3^-, indicated by the left superscript b, in the four regions are given by

$$\begin{aligned}\frac{\partial {}^{b}C_{rbc}}{\partial t} = &-\frac{F_{rbc}L}{V_{rbc}}\frac{\partial {}^{b}C_{rbc}}{\partial x}\\ &-\frac{{}^{b}PS_{rbc}}{V'_{rbc}}({}^{b}C_{rbc} - R_{rbc}\,{}^{b}C_{pl}) + {}^{b}D_{rbc}\frac{\partial^2 {}^{b}C_{rbc}}{\partial x^2}\\ &+ K_{rbc}(kf_1\,{}^{c}C_{rbc} - kb_1\,{}^{b}C_{rbc}\,{}^{h}C_{rbc}),\end{aligned} \tag{12a}$$

$$\begin{aligned}\frac{\partial {}^{b}C_{pl}}{\partial t} = &-\frac{F_{pl}L}{V_{pl}}\frac{\partial {}^{b}C_{pl}}{\partial x} + \frac{{}^{b}PS_{rbc}}{V'_{pl}}({}^{b}C_{rbc} - R_{rbc}\,{}^{b}C_{pl})\\ &-\frac{{}^{b}PS_{cap}}{V'_{pl}}(R_{cap}\,{}^{b}C_{pl} - {}^{b}C_{isf}) + {}^{b}D_{pl}\frac{\partial^2 {}^{b}C_{pl}}{\partial x^2}\\ &+ K_{pl}(kf_1\,{}^{c}C_{pl} - kb_1\,{}^{b}C_{pl}\,{}^{h}C_{pl}),\end{aligned} \tag{12b}$$

$$\begin{aligned}\frac{\partial {}^{b}C_{isf}}{\partial t} = &\frac{{}^{b}PS_{cap}}{V'_{isf}}(R_{cap}\,{}^{b}C_{pl} - {}^{b}C_{isf}) - \frac{{}^{b}PS_{pc}}{V'_{isf}}(R_{pc}\,{}^{b}C_{isf}\\ &- {}^{b}C_{pc}) + {}^{b}D_{isf}\frac{\partial^2 {}^{b}C_{isf}}{\partial x^2}\\ &+ K_{isf}(kf_1\,{}^{c}C_{isf} - kb_1\,{}^{b}C_{isf}\,{}^{h}C_{isf}),\end{aligned} \tag{12c}$$

$$\begin{aligned}\frac{\partial {}^{b}C_{pc}}{\partial t} = &\frac{{}^{b}PS_{pc}}{V'_{pc}}(R_{pc}\,{}^{b}C_{isf} - {}^{b}C_{pc}) + {}^{b}D_{pc}\frac{\partial^2 {}^{b}C_{pc}}{\partial x^2}\\ &+ K_{pc}(kf_1\,{}^{c}C_{pc} - kb_1\,{}^{b}C_{pc}\,{}^{h}C_{pc}).\end{aligned} \tag{12d}$$

As for the CO_2 equations, the last terms in Eqs. (12a)–(12d) represent the net rate of formation of HCO_3^-, and are the same as the last terms in Eqs. (8a)–8d.

Equations for Hydrogen Ions and Acid–Base Balance

Because the reactions of O_2 and CO_2 with Hb, Mb, and HCO_3^- are influenced greatly by variation in pH,[26] the transport and exchange of hydrogen ions (H^+) must be incorporated into any model for O_2, CO_2, and HCO_3^-. Variation in pH due to the CO_2 hydration reaction is controlled by the buffering action of bicarbonate (HCO_3^-) in both blood and tissue. It is characterized by the buffering capacity parameter, β, which is the amount of base added, or equivalently acid removed, per unit pH change: $\beta = +\Delta[\text{base}]/\Delta\text{pH} = -\Delta[\text{acid}]/\Delta\text{pH}$. Here, the acid is H_2CO_3 (carbonic acid) and the base is HCO_3^-. As for HCO_3^-, the exchange of H^+ through the band-3 proton channels at equilibrium or steady state is governed by the Gibbs–Donnan electrochemical equilibrium conditions: Eqs. (1a)–(1c). The four-region equations are

$$\begin{aligned}\frac{\partial {}^{h}C_{rbc}}{\partial t} = &-\frac{F_{rbc}L}{V_{rbc}}\frac{\partial {}^{h}C_{rbc}}{\partial x} - \frac{{}^{h}PS_{rbc}}{V'_{rbc}}(R_{rbc}\,{}^{h}C_{rbc} - {}^{h}C_{pl})\\ &+ {}^{h}D_{rbc}\frac{\partial^2 {}^{h}C_{rbc}}{\partial x^2} + \frac{2.303}{\beta_{rbc}}K_{rbc}\,{}^{h}C_{rbc}(kf_1\,{}^{c}C_{rbc}\\ &- kb_1\,{}^{b}C_{rbc}\,{}^{h}C_{rbc}),\end{aligned} \tag{13a}$$

$$\frac{\partial {}^{h}C_{pl}}{\partial t} = -\frac{F_{pl}L}{V_{pl}}\frac{\partial {}^{h}C_{pl}}{\partial x} + \frac{{}^{h}PS_{rbc}}{V'_{pl}}(R_{rbc}\,{}^{h}C_{rbc} - {}^{h}C_{pl})$$

$$- \frac{{}^{\mathrm{h}}PS_{\mathrm{cap}}}{V'_{\mathrm{pl}}}({}^{\mathrm{h}}C_{\mathrm{pl}} - R_{\mathrm{cap}}{}^{\mathrm{h}}C_{\mathrm{isf}}) + {}^{\mathrm{h}}D_{\mathrm{pl}}\frac{\partial^{2\mathrm{h}}C_{\mathrm{pl}}}{\partial x^2}$$
$$+ \frac{2.303}{\beta_{\mathrm{pl}}}K_{\mathrm{pl}}{}^{\mathrm{h}}C_{\mathrm{pl}}(kf_1{}^{\mathrm{c}}C_{\mathrm{pl}} - kb_1{}^{\mathrm{b}}C_{\mathrm{pl}}{}^{\mathrm{h}}C_{\mathrm{pl}}), \quad (13b)$$

$$\frac{\partial^{\mathrm{h}}C_{\mathrm{isf}}}{\partial t} = \frac{{}^{\mathrm{h}}PS_{\mathrm{cap}}}{V'_{\mathrm{isf}}}({}^{\mathrm{h}}C_{\mathrm{pl}} - R_{\mathrm{cap}}{}^{\mathrm{h}}C_{\mathrm{isf}}) - \frac{{}^{\mathrm{h}}PS_{\mathrm{pc}}}{V'_{\mathrm{isf}}}({}^{\mathrm{h}}C_{\mathrm{isf}}$$
$$- R_{\mathrm{pc}}{}^{\mathrm{h}}C_{\mathrm{pc}}) + {}^{\mathrm{h}}D_{\mathrm{isf}}\frac{\partial^{2\mathrm{h}}C_{\mathrm{isf}}}{\partial x^2} + \frac{2.303}{\beta_{\mathrm{isf}}}K_{\mathrm{isf}}$$
$${}^{\mathrm{h}}C_{\mathrm{isf}}(kf_1{}^{\mathrm{c}}C_{\mathrm{isf}} - kb_1{}^{\mathrm{b}}C_{\mathrm{isf}}{}^{\mathrm{h}}C_{\mathrm{isf}}), \quad (13c)$$

$$\frac{\partial^{\mathrm{h}}C_{\mathrm{pc}}}{\partial t} = \frac{{}^{\mathrm{h}}PS_{\mathrm{pc}}}{V'_{\mathrm{pc}}}({}^{\mathrm{h}}C_{\mathrm{isf}} - R_{\mathrm{pc}}{}^{\mathrm{h}}C_{\mathrm{pc}}) + {}^{\mathrm{h}}D_{\mathrm{pc}}\frac{\partial^{2\mathrm{h}}C_{\mathrm{pc}}}{\partial x^2}$$
$$+ \frac{2.303}{\beta_{\mathrm{pc}}}K_{\mathrm{pc}}{}^{\mathrm{h}}C_{\mathrm{pc}}(kf_1{}^{\mathrm{c}}C_{\mathrm{pc}}$$
$$- kb_1{}^{\mathrm{b}}C_{\mathrm{pc}}{}^{\mathrm{h}}C_{\mathrm{pc}}) \, . \quad (13d)$$

where β_{rbc}, β_{pl}, β_{isf}, and β_{pc} (with units M pH^{-1} unit) are the buffering capacities in the four regions of the BTEX unit; β_{pl} is small, but β_{rbc}, β_{isf}, and β_{pc} are high; we choose $\beta_{\mathrm{pl}} = 6$ mM pH^{-1} unit, $\beta_{\mathrm{rbc}} = 54$ mM pH^{-1} unit, $\beta_{\mathrm{isf}} = 24$ mM pH^{-1} unit, and $\beta_{\mathrm{pc}} = 45$ mM pH^{-1} unit from Hill *et al.*[39–41] Salathe *et al.*,[58] and Huang and Hellums.[44]

Equations for Capillary Hematocrits and RBC and Plasma Volumes

The capillary hematocrits ($\mathrm{Hct}_{\mathrm{cap}}$) are lower than the large-vessel hematocrits (Hct) by the Fahraeus–Lindquist effect[3,32,43] and consequently the RBC velocity (v_{rbc}) is higher than the plasma velocity (v_{pl}), and the erythrocytes' mean transit times through the coronary system is shorter than that of plasma.[9] The result is a "red cell carriage effect"[33] whereby solutes carried within RBCs travel faster than plasma proteins. In this model, Hct, blood flow (F_{bl}), capillary volume (V_{cap}), and the ratio of RBC to plasma velocity (R_{vel}) are known. The standard values for myocardial blood flow are $\mathrm{Hct} = 0.45$, $F_{\mathrm{bl}} = 1$ ml min^{-1} g^{-1}, $V_{\mathrm{cap}} = 0.07$ ml g^{-1}, and $R_{\mathrm{vel}} = 1.6$. The $\mathrm{Hct}_{\mathrm{cap}}$, RBC and plasma flows ($F_{\mathrm{rbc}}$ and F_{pl}), their volumes (V_{rbc} and V_{pl}), and their velocities (v_{rbc} and v_{pl}) are calculated through the following equations,[51] the values of which are presented in Table 1 for standard physiological conditions:

$$F_{\mathrm{rbc}} = \mathrm{Hct}\ F_{\mathrm{bl}} \quad \text{and} \quad F_{\mathrm{pl}} = (1 - \mathrm{Hct})\ F_{\mathrm{bl}}, \quad (14a)$$

$$V_{\mathrm{rbc}} = \mathrm{Hct}_{\mathrm{cap}}\, V_{\mathrm{cap}} \quad \text{and} \quad V_{\mathrm{pl}} = (1 - \mathrm{Hct}_{\mathrm{cap}})\, V_{\mathrm{cap}}, \quad (14b)$$

$$R_{\mathrm{vel}} = \frac{v_{\mathrm{rbc}}}{v_{\mathrm{pl}}}, \quad v_{\mathrm{rbc}} = \frac{F_{\mathrm{rbc}}L}{V_{\mathrm{rbc}}}, \quad \text{and} \quad v_{\mathrm{pl}} = \frac{F_{\mathrm{pl}}L}{V_{\mathrm{pl}}}, \quad (14c)$$

$$\mathrm{Hct}_{\mathrm{cap}} = \frac{\mathrm{Hct}}{\mathrm{Hct} + (1 - \mathrm{Hct})R_{\mathrm{vel}}} \, . \quad (14d)$$

The water fractions of various spaces are given by $W_{\mathrm{pl}} = 0.94$, $W_{\mathrm{rbc}} = 0.72$, $W_{\mathrm{isf}} = 0.92$, $W_{\mathrm{pc}} = 0.8$.[51] The anatomical volumes of ISF and parenchymal cells are given by $V_{\mathrm{isf}} = 0.2$ ml g^{-1} and $V_{\mathrm{pc}} = 0.7$ ml g^{-1}, so the water spaces or volumes of distribution of these two regions are about 0.18 and 0.56 ml g^{-1}.[9]

Steady-State Extraction and the Consumption Rate of Oxygen

The fractional steady-state extraction of O_2 (E_{ss}) and its consumption rate ($\mathrm{MR}_{\mathrm{O_2}}$) can be obtained from total O_2 content in the arterial and venous blood ($^{\circ}C_{\mathrm{Tot\,Art}}$): and $^{\circ}C_{\mathrm{Tot\,Ven}}$):

$$E_{\mathrm{ss}} = \frac{{}^{\circ}C_{\mathrm{TotArt}} - {}^{\circ}C_{\mathrm{TotVen}}}{{}^{\circ}C_{\mathrm{TotArt}}},$$
$$\mathrm{MR}_{\mathrm{O_2}} = F_{\mathrm{bl}}({}^{\circ}C_{\mathrm{TotArt}} - {}^{\circ}C_{\mathrm{TotVen}}) \, , \quad (15)$$

where

$${}^{\circ}C_{\mathrm{TotArt,\,TotVen}} = [(1 - \mathrm{Hct})W_{\mathrm{pl}}{}^{\circ}C_{\mathrm{pl}}$$
$$+ \mathrm{Hct}W_{\mathrm{rbc}}({}^{\circ}C_{\mathrm{rbc}} + C_{\mathrm{HbO_2}})]\Big|_{x=\mathrm{Art,\,Ven}} \quad (16)$$

The $\mathrm{MR}_{\mathrm{O_2}}$ in Eq. (15) equals the integral of ${}^{\circ}G_{\mathrm{pc}}{}^{\circ}C_{\mathrm{pc}}$ over the axial length L in Eq. (2d).

Computational Methods

To obtain the solutions for concentration profiles, one must prescribe initial and boundary conditions for the governing partial differential equations (2a)–(2d), (8a)–(8d), (12a)–(12d), and (13a)–(13d). For equilibrium/steady-state solutions, the initial conditions are chosen arbitrarily, ${}^{\mathrm{s}}C_{\mathrm{r}}(x, t) = {}^{\mathrm{s}}C_{\mathrm{r0}}(x)$; the boundary conditions are derived from the physiological conditions prevailing at arterial and venous ends. In flowing RBC and plasma regions, the conditions are given by

$${}^{\mathrm{s}}C_{\mathrm{r}} = {}^{\mathrm{s}}C_{\mathrm{art}} \quad \text{at} \quad x = 0$$
$$\text{and} \quad \partial {}^{\mathrm{s}}C_{\mathrm{r}}/\partial x = 0 \quad \text{at} \quad x = L \, , \quad (17)$$

where ${}^{\mathrm{s}}C_{\mathrm{art}}$ is the concentration of the species 's' (O_2, CO_2, HCO_3^-, and H^+) in the inflowing arterial blood, where plasma and RBC solutes are assumed to have equilibrated prior to entry into the exchange region at $x = 0$. These can be computed from standard arterial P_{O_2}, P_{CO_2}, and pH (see Table 1). The concentration of HCO_3^- at the arterial end is obtained using the Henderson–Hasselbach equation and Gibbs–Donnan electrochemical equilibrium condition.[26] In non-flowing ISF and parenchymal cell regions, the boundary conditions are the no-flux (reflecting)

conditions that are given by

$$\partial^{s} C_{r}/\partial x = 0 \quad \text{at} \quad x = 0 \quad \text{and} \quad x = L. \qquad (18)$$

The model is coded and run in the JSim model simulation environment[23] and is solved by invoking either the LSFEA (Lagrangian Sliding Fluiding Element Algorithm,[13]) or TOMS690 Chebychev Polynomial Algorithm[19] or TOMS731 Moving-Grid Algorithm[21] from our library of numerical PDE solvers. LSFEA is the fastest of these, even though accurate solutions at the inlet require a finer grid or number of axial segments than do the TOMS algorithms.[13] In contrast, TOMS731 is considerably faster than TOMS690, and the solutions are equally accurate. All the results presented in this paper were obtained using the TOMS731 solver with 51 axial grid points. The time step of integration is adaptively controlled by the solver. The solver computes the concentrations of total O_2 in RBC and parenchymal cells ($^{\circ}C_{rbc} + C_{HbO_2}$ and $^{\circ}C_{pc} + C_{MbO_2}$) and total CO_2 in RBC ($^{c}C_{rbc} + C_{HbCO_2}$) at each axial grid point at each time point. The concentrations of free O_2 in RBC and parenchymal cells ($^{\circ}C_{rbc}$ and $^{\circ}C_{pc}$) and free CO_2 in RBC ($^{c}C_{rbc}$) are then obtained iteratively from the coupled Eqs. (4), (5), (9), and (10).

This model's capabilities extend those of the previous models,[20,27,51,55] and it is computationally fast in spite of its comprehensive nature, so this model is our preferred vehicle for data analysis for oxygen-related studies, for example for ^{15}O-oxygen studies using positron emission tomography where many regions of interest are analyzed within an organ. The model is available for download and public use from the Physiome website at http://physiome.org/Models/GasTransport/o2co2btex.proj/.

RESULTS: MODEL BEHAVIOR AND FUNCTIONALITY

The Default Parameter Set

The model requires many parameters, and while there are many sources for partial information, it has not been possible to find a consistent set of values in the literature. Consequently, a self-consistent set of parameter values were chosen to represent realistic normal physiological conditions; as listed in Table 1 with references. Where the value of a parameter was not available, known relationships to other parameters (correlation) were used to constrain the missing parameter value. When applying the model to data analysis or simply making predictions from the model, the aim is to fix the values for as many parameters as possible, and thereby to minimize the degrees of freedom for data fitting or exploring behavior under varying physiological conditions. Known physicochemical parameters can be fixed. Anatomic parameters can often be fixed or markedly constrained using data coming from other experiments than the one being analyzed; parameters for which there is low sensitivity, e.g., cell volumes and water spaces, fit into this category.[65] In fitting the model to actual experimental data (e.g., tracer-dilution outflow curves following the injection of tracer-labeled ^{15}O-oxygen in PET imaging studies) to estimate the physiological parameters of particular interest, oxygen consumption, the RQ, or response times for a change in metabolism, all but a few parameters need to be determined by optimization to fit data.[27,51]

With Table 1's parameter values, the effects of blood flow, hematocrits, arterial P_{O_2}, and oxygen consumption on the concentration profiles can be studied by changing parameter values one at a time, a kind of sensitivity analysis. The results presented later in Figs. 2–6, give a portrayal of the model functions and the model's utility in exploring physiological interventions.

Axial Profiles at Standard Physiological Conditions

The computed steady-state axial profiles for O_2, CO_2, HCO_3^-, and H^+ in the four regions of the blood–tissue exchange unit using the standard parameter values presented in Table 1 are shown in Fig. 2. The local $^{o}G_{pc}$ at each x is defined by Eq. (7). Oxygen P_{O_2} (*left upper*) decays along the capillary, while the concentrations of metabolic products are all rising, P_{CO_2} (*right upper*), bicarbonate [HCO_3^-] (*left lower*), and H^+ ion (*right lower*), in all four regions (RBC, plasma, ISF, and parenchymal cells). The arterial inflow concentrations were constant at $P_{O_2} = 100$ mmHg, $P_{CO_2} = 40$ mmHg, $pH_{pl} = 7.4$, $pH_{rbc} = 7.24$, $[HCO_3^-]_{pl} = 24.4$ mM, and $[HCO_3^-]_{rbc} = 16.8$ mM. In the venous outflow, the computed solutions were $P_{O_2} = 39$ mmHg, $P_{CO_2} = 46.5$ mmHg, $pH_{pl} = 7.36$, $pH_{rbc} = 7.2$, $[HCO_3^-]_{pl} = 26.4$ mM, and $[HCO_3^-]_{rbc} = 18.2$ mM. These simulated results are in good agreement with the literature and standard physiological observations (e.g., see Huang and Hellums[37] and Hellums *et al.*[44]).

Figure 2 shows steep gradients in O_2, more or less exponentially decaying, while the increasing concentrations in CO_2, HCO_3^-, and H^+ show considerably smaller gradients because they are heavily buffered. In contrast to the exponential decay in dissolved free O_2 concentration, the Hb-bound O_2 concentration decays very nearly linearly from a saturation, $S_{HbO_2} = 0.98$ at the entrance to $S_{HbO_2} = 0.74$ at the exit. This is due to the nonlinear (sigmoid) nature of the oxyhemoglobin dissociation curve and nonlinear–nonlinear interaction of sigmoid–exponential curves. The trend in Hb-bound CO_2 concentration was opposite, though $HbCO_2$ increased only slightly along the capillary length. The steady-state O_2 extraction at the venous end was 25.4%. The average intracellular O_2 consumption, MR_{O_2}, was under these conditions equal to V_{max}, 2.5 μ mol min^{-1}g^{-1}, so the intracellular O_2 level was sufficient to saturate the cytochrome-c and to put cellular respiration into the zero-order mode, nearly constant at all positions along the BTEX unit. The [O_2] in RBC and plasma as well as in ISF and

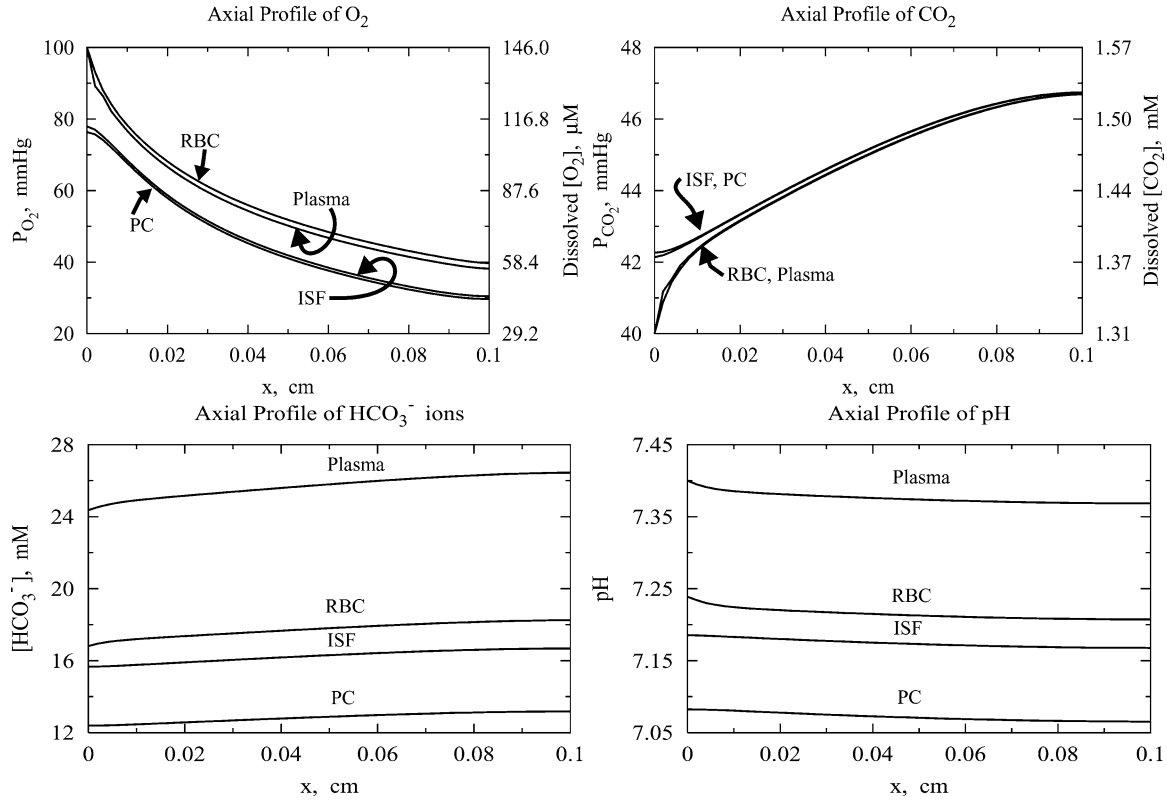

FIGURE 2. The simulated steady-state axial profiles of O_2, CO_2, HCO_3^-, and H^+ in the four regions of the BTEX unit at standard physiological conditions for which the parameter values are presented in Table 1. Axial dispersion coefficients (^sD_r) for all species in all regions were assigned the value 1×10^{-4} cm^2 s^{-1}. $V_{max} = 2.5$ μmol min^{-1} g^{-1} and $K_m = 7.7 \times 10^{-7}$ M.

parenchymal cells were close to each other, indicating the RBC and plasma as well as ISF and parenchymal cells regions were equilibrated with O_2. However, even with $^\circ PS_{cap}$ at the rather high value of 200 ml g^{-1} min^{-1} there was an $[O_2]$ gradient across the capillary wall, which no experimental evidence has either corroborated or contradicted, suggesting that this permeability is underestimated. In contrast, $[CO_2]$ was in close equilibrium in all four regions of the blood–tissue exchange unit (except near the arterial end), as there was negligible gradient in $[CO_2]$ across the membranes. The $[HCO_3^-]$ and $[H^+]$ were found to vary negligibly in axial direction (probably due to the

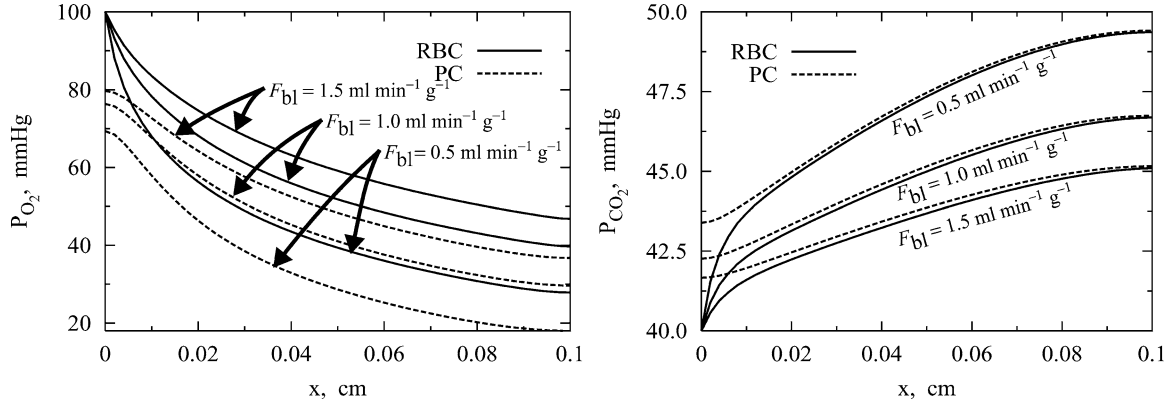

FIGURE 3. Effect of varying capillary blood flow (F_{bl}) on steady-state axial profiles of O_2 and CO_2 (P_{O_2} and P_{CO_2}) in RBC and parenchymal cell (PC) regions of the BTEX unit. Inflow P_{O_2} and P_{CO_2} were fixed at 100 and 40 mmHg. Axial dispersion coefficients were fixed at 10^{-4} cm^2 s^{-1}. $V_{max} = 2.5$ μmol min^{-1} g^{-1}.

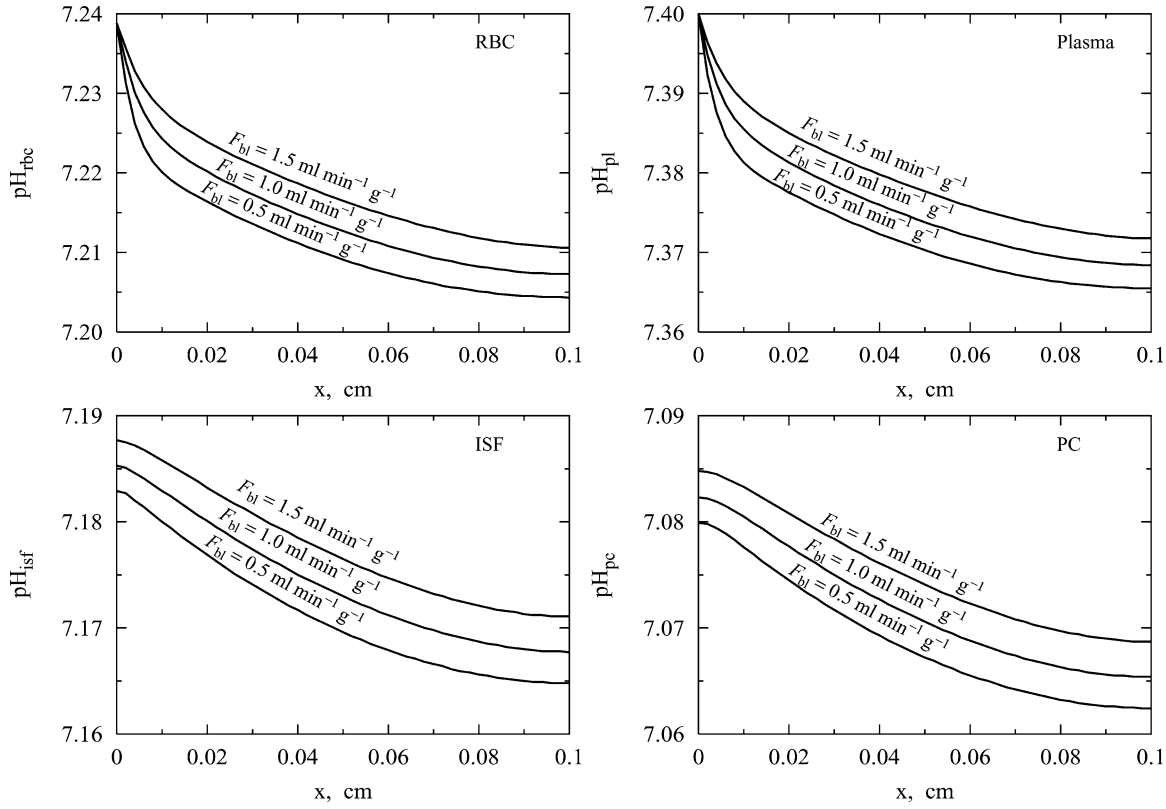

FIGURE 4. Effect of varying capillary blood flow (F_{bl}) on the steady-state axial profile of H^+ ions (pH) in the four regions of the BTEX unit. Inflow pH_{rbc} and pH_{pl} were fixed at 7.24 and 7.4. Axial dispersion coefficients were fixed at 10^{-4} cm^2 s^{-1}. V_{max} = 2.5 μmol min^{-1} g^{-1}.

buffering action of HCO_3^-) and were in equilibrium in different regions obeying the Gibbs–Donnan electrochemical equilibrium conditions given by Eqs. (1a)–(1c). The pH inside the parenchymal cells, driven by the production of CO_2 in this oversimplified model of metabolism, is too low compared to observed pHs in normal myocardium, simply because there is no representation of H^+ ion consumption by the processes of oxidative metabolism in the model. This lack reduces all regional pHs compared to those for a fully-developed metabolic model.

Effect of Varying Blood Flow, Hematocrit, and Arterial P_{O_2} on Axial Profiles

The delivery of O_2 to the tissue is determined mainly by three factors: Capillary blood flow, hematocrit, and arterial P_{O_2}. These also affect the axial profiles of O_2, CO_2, HCO_3^-, and H^+. All these have similar qualitative effects and can be explained from the behavior of one of the factors. The effect of varying capillary blood flow (F_{bl}) on steady-state axial profiles of O_2, CO_2, and H^+ in the four regions of the blood–tissue exchange unit are shown in Figs. 3 and 4. Other parameters, including the conditions at the arterial end, are fixed at the standard physiological values presented in Table 1. The steady-state axial profiles of HCO_3^- (not shown) can be deduced from the steady-state axial profiles of P_{CO_2} and pH (using the Henderson–Hasselbalch equation). Figure 3 actually shows the steady-state axial variations of P_{O_2} and P_{CO_2} in RBC and parenchymal cells for F_{bl} = 1.5, 1.0, 0.5 ml min^{-1} g^{-1}. The profiles of P_{O_2} and P_{CO_2} in plasma and ISF are not included in these plots because these profiles almost match with those in RBC and parenchymal cells. Figure 4 shows the steady-state axial profile of pH in RBC, plasma, ISF, and parenchymal cells for the same three values of F_{bl}.

It is seen that as the capillary blood flow (perfusion or O_2 supply) decreases with the O_2 consumption, while V_{max} (O_2 demand) remains constant, the concentration of O_2 in the blood–tissue exchange unit decreases. However, the P_{O_2} does not go to zero anywhere. With arterial P_{O_2} = 100 mmHg, V_{max} = 2.5 μ mol min^{-1} g^{-1}, and F_{bl} = 1.5, 1.0, 0.5 ml min^{-1} g^{-1}, we see that the venous P_{O_2} is 46, 39, 27 mmHg and O_2 extraction is 17.3, 25.4, 48.1%. A decrease in blood flow also results in an increase in the concentrations of CO_2, H^+, and HCO_3^- in the system. Thus, a severe blood flow decrease (ischemia) can result in acute hypoxia and acidosis (lower pH) inside the parenchymal cells and affect the normal cellular function.

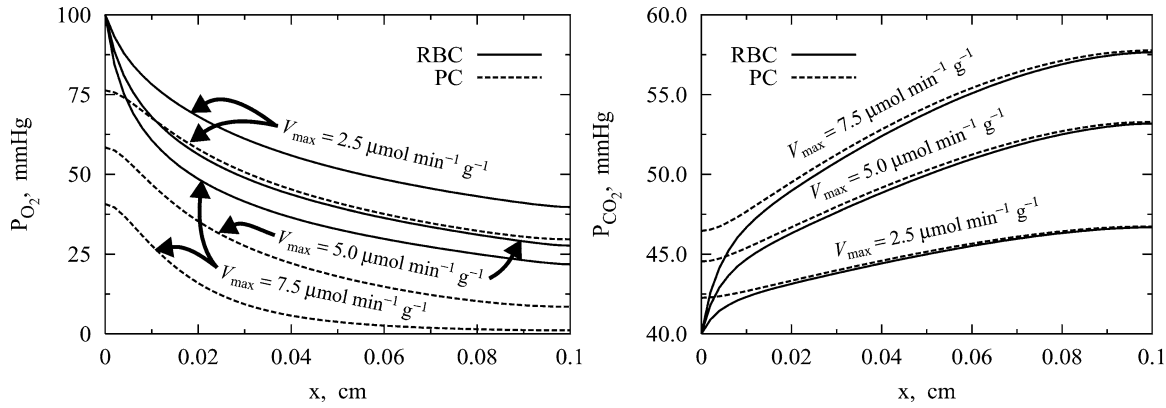

FIGURE 5. Effect of varying O_2 consumption V_{max} on steady-state axial profiles of O_2 and CO_2 (P_{O_2} and P_{CO_2}) in RBC and parenchymal cell (PC) regions of the BTEX unit. Inflow P_{O_2} and P_{CO_2} were fixed at 100 and 40 mmHg. Axial dispersion coefficients were fixed at 10^{-4} cm^2 s^{-1}. F_{bl} = 1 ml min^{-1} g^{-1}.

Effect of Varying Oxygen Consumption on Axial Profiles

The effect of varying O_2 consumption V_{max} on steady-state axial profiles O_2, CO_2, and H^+ in the four regions of the blood–tissue exchange unit is shown in Figs. 5 and 6. Other parameters, including the conditions at the arterial end, are fixed at the standard physiological values presented in Table 1. Figure 5 shows the steady-state axial variations of P_{O_2} and P_{CO_2} in RBC and parenchymal cells for V_{max} = 2.5, 5.0, 7.5 μmol min^{-1} g^{-1}. Figure 6 shows the steady-state axial variation of pH in RBC, plasma, ISF, and parenchymal cells for the same three values of V_{max}. These results are consistent with the results in Figs. 3 and 4, i.e., the increasing O_2 consumption V_{max} (O_2 demand) has similar qualitative effects on the species concentration profiles as does decreasing capillary blood flow (perfusion or O_2 supply). Both cause decreases in the regional O_2 concentration and increases in the regional concentrations of CO_2, H^+, and HCO_3^- in the system. Quantitatively the differences between the regional concentration profiles are larger with varying V_{max} than with varying F_{bl}, using the same relative increments, comparing Fig. 6 with Fig. 4. With arterial P_{O_2} = 100 mmHg, F_{bl} = 1 ml min^{-1} g^{-1}, and V_{max} = 2.5, 5.0, 7.5 μmol min^{-1} g^{-1}, the venous P_{O_2} is seen to vary from 39 to 26 to 20 mmHg and O_2 extraction is seen to vary from 25.4 to 50.2 to 66.8%. With V_{max} = 5.0 μmol min^{-1} g^{-1} the downstream end of the parenchymal cells has a P_{O_2} of 10 mmHg and pH of 7.03. With V_{max} = 7.5 μmol min^{-1} g^{-1}, the downstream half of the parenchymal cells has a P_{O_2} < 5 mmHg and pH of 7.01. Therefore, when there is an increasing energy demand and O_2 consumption (associated with exercise), unless the capillary blood flow and O_2 supply increase to meet the energy demand, the normal cellular function will be severely affected.

It may be noted here that in acute situations with very low blood flow (F_{bl}) or very high oxygen consumption (V_{max}) the blood P_{O_2} can become very low (below 20 mmHg) in the downstream end of the blood–tissue exchange region, and the HbO_2 saturation will fall below 30%. Our model for HbO_2 saturation[26] begins to lose accuracy below S_{HbO} = 30%, so the computed solutions are less accurate in this regime of low P_{O_2}.

DISCUSSION AND CONCLUDING REMARKS

Potential Applications

This model is the start of, or a part of, whole-body metabolic modeling for systems physiology. While it encompasses only the simultaneous transport and exchanges of O_2, CO_2, HCO_3^-, and H^+ in the microcirculation, it links these processes to the metabolism of O_2 and therefore to the whole realm of intracellular metabolism. Augmenting such a model by adding biochemical systems for intermediary metabolism, oxidative phosphorylation, NAD/NADH reactions, the tricarboxylic acid cycle, and hydrogen balance will improve the characterization of spatial profiles and representation of kinetics during transients. Through whole-body representation of multiple organs, such a model can be expanded into a model for glucose metabolism, for example.

The model itself is worthwhile as a basic vehicle for data analysis for whole-organ studies by multiple indicator dilution techniques, by positron emission tomographic or NMR image sequences. For application to BOLD (blood oxygen level dependent) NMR, one has only to pull out the signal for Hb rather than HbO [where HbO really represents $Hb(O_2)_4$]. As a component of a model further developed to include mitochondrial oxygen and carbon dioxide kinetics, and linked into a whole-organ model by adding the arterial and venous transport systems, one will be able to evaluate the basis for the delays in responses to changes in oxygen utilization with changes in cardiac contractile performance.

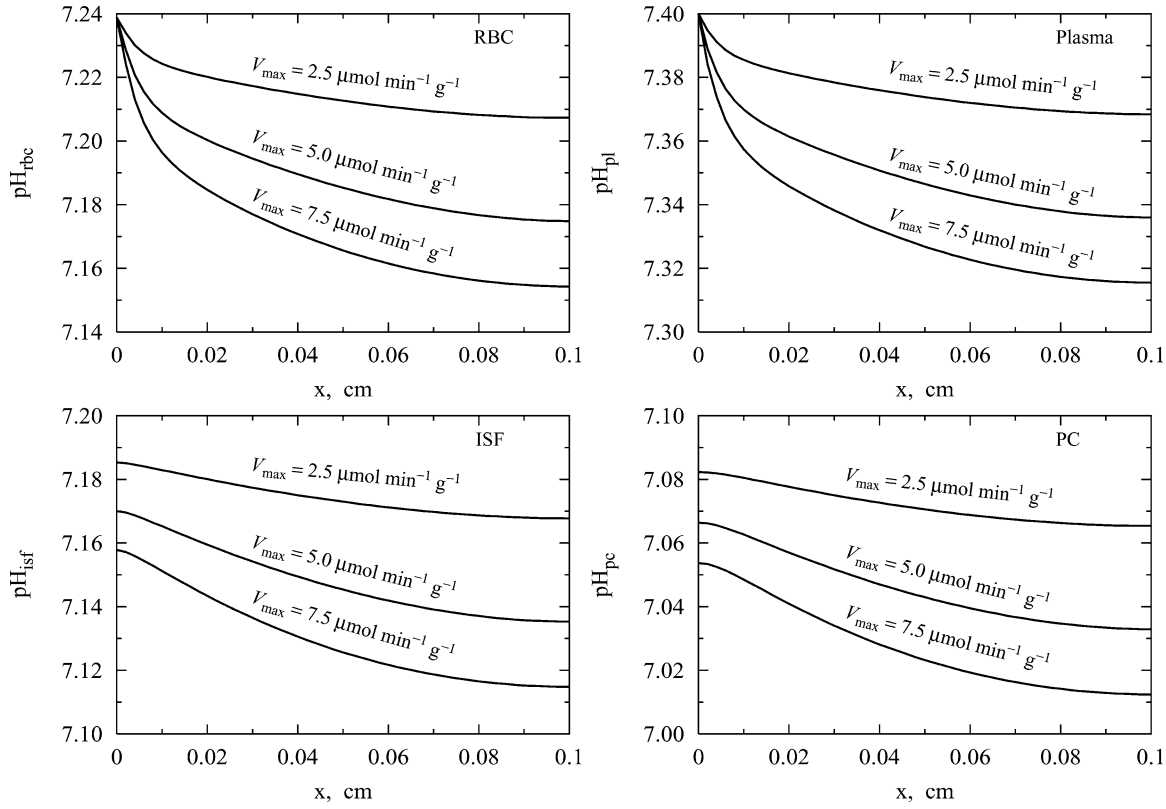

FIGURE 6. Effect of varying O_2 consumption V_{max} on the steady-state axial profile of H^+ ions (pH) in the four regions of the BTEX unit. Inflow pH_{rbc} and PH_{pl} were fixed at 7.24 and 7.4. Axial dispersion coefficients were fixed at 10^{-4} cm^2 s^{-1}. F_{bl} = 1 ml min^{-1} g^{-1}.

This has been a puzzle: "Is it mitochondrial delay or is it merely a transport time?"

What is modeled here has been well known for years, but the complexity of the problem and the slowness of computation inhibited developing full sets of equations for practical applications. The model is free for general use and available for download. Investigators anywhere can explore the model behavior with or without delving into the code by going to the website for JSim.[23] This fits with current trends toward open-source software and widespread collaboration in research. Models including the O_2–CO_2 interactions were presented by Huang and Hellums[44] and Ye *et al.*,[67] but for different reasons neither of their approaches lends itself to the quantitative analysis of experimental data from transients in venous P_{O_2} or tracer ^{15}O-oxygen in positron emission tomography (PET) imaging studies. The model of[44] accounts for radial diffusion, but is computationally slow, making it impractical for routine fitting of experimental time courses from PET imaging studies by automated iterative parameter adjustment optimization. The model of Ye *et al.*[67] was compartmental, thereby failing to account for axial gradients along the capillary, and therefore lacking the critical narrow impulse response required to fit high-resolution data of the sort analyzed by Deussen and Bassingthwaighte[27] and Li *et al.*[51] The current model solves the first of these problems by an approximation (for radial diffusion) and by using highly efficient computational algorithms for Hb/HbO and for the blood–tissue exchange, and the second by using very efficient partial rather than ordinary differential equations.

This general model can readily be applied to arterioles and venules and to other organs (e.g., the lungs) for gaining insight into the processes of O_2 and CO_2 transport and exchange as well as acid–base regulation along the length of the microcirculatory exchange regions from arterioles to venules.

Improvements Over Prior Models

The current model improves our previous blood–tissue exchange models of O_2 transport and metabolism[20,27,51] for it uses the analytically invertible expressions of Dash and Bassingthwaighte[26] for oxyhemoglobin (HbO_2) and carbamino hemoglobin ($HbCO_2$) dissociation curves which explicitly account for the effects of P_{O_2}, P_{CO_2}, pH, and nonlinear O_2–CO_2 interactions in computing P_{O_2} and P_{CO_2} from the total O_2 and CO_2 concentrations ($^{\circ}C_{rbc} + C_{HbO_2}$ and $^{c}C_{rbc} + C_{HbCO_2}$) in RBC at each axial and time grid point. This reduces the computation time by about a factor of 20 compared to solving the Adair-type equations by iteration.[26]

Computational efficiency is a major issue in analyzing the data from PET imaging studies of tracer-labeled ^{15}O-oxygen because of the broad heterogeneity of flows and metabolism in the heart (e.g., see King *et al.*,[47] Caldwell *et al.*,[24] reviews by Bassingthwaighte *et al.*[14] The steady-state spatial distribution of regional blood flows within organs is always broad, having coefficients of variation of 25% or more, depending on the tissue under study and the ambient humoral, nervous, and metabolic conditions.[9,47] To allow an approximate description of spatial heterogeneity at the level of spatial resolution of about 0.5–1% of the heart mass (the resolution used for PET analysis) and still account for the heterogeneity within the observed region-of-interest, our capillary–tissue exchange model can be incorporated into a multicapillary configuration in which the blood–tissue exchange regions are composed of a set of parallel, independent capillary–tissue exchange units such as those described.[27,48]

The O_2 consumption in such small tissue regions can be measured directly using the tracer kinetics of ^{15}O-oxygen in PET imaging[51] and in isolated perfused rabbit hearts.[27] For standard PET imaging data analysis, one uses 30–100 regions of interest within the LV myocardium, so efficiency is very important. To extend our current nontracer model for the analysis of tracer ^{15}O-oxygen from PET imaging studies, it needs to be integrated with an identical model for tracer ^{15}O-oxygen and its product, tracer ^{15}O-water, which is formed in the mitochondria. The steady-state solutions of the current model will provide the volumes of distribution (virtual volumes) for the tracer ^{15}O-oxygen that accounts for the Hb binding space and water space. The current model differs from that of Li *et al.*[51] in the sense that the virtual volumes will be functions of P_{O_2}, P_{CO_2}, and pH, and therefore will vary under varying physiological conditions.

Assessment of the Model's Features

As reviewed in detail by Hellums *et al.*,[37] there are a number of issues to be addressed in any integrated model that contains simplifications or approximations of the real geometry and physiology. These issues include (1) the exchanges across the arterioles and venules walls and the complexity of diffusional interactions among the capillaries, arterioles, and venules, (2) the radial gradients in blood, particularly in arterioles and venules, and in tissues, (3) the increase in intracapillary diffusional resistance due to the spacings between RBC in the capillary, (4) the existence of a continuous disequilibrium between O_2 and Hb and between O_2 and Mb during steady states involving diffusion and consumption (and likewise for CO_2 with Hb), (5) the anion exchanges (HCO_3^- and Cl^-) across the membranes, and (6) at the level of molecular interactions, the release of approximately 0.7 H^+ and binding of 60 H_2O molecules[25] when O_2 binds to Hb.

The components of Issue 1, arteriolar and venular exchanges, can be handled approximately, using three or more BTEX units in series, as was done.[27] The first serves as the arteriole, the second as the capillary–tissue region and the third as the venule. The parameters for the volumes and permeabilities of the arteriolar and venular sections are adjusted to match reality. The resistances between blood and tissue are the sum of those of the vessel walls (with a minor degree of O_2 consumption by the smooth muscle and other cells) and of the loose aureolar connective tissue surrounding the vessels and allowing their expansion and contraction. Further, the arrangement in many tissues including the heart where each arteriole is accompanied by two venules (*venae comitantes*[6]) means that some oxygen diffuses from arterioles to interstitium to venules without passing by the muscle cells. While this is most obvious for heat exchange,[9] it is a major factor in shaping the impulse responses for tracer water[16] and oxygen[17]; this can be accounted for, again approximately but rather well, by increasing the D_{isf}, the dispersion coefficient in the interstitial fluid space, to allow graded fluxes between the upstream and downstream ends of the capillary–tissue exchange unit, which accounts approximately for the asynchrony or offsettedness of capillary entrances and exits. An improved treatment would include the arterio-venous exchanges directly in addition to the dispersion.

Compensating for the omission of radial gradients (Issue 2) is important. O_2 and CO_2 gradients will be poorly represented in arterioles and venules. Radial diffusion in 20–40-micron diameter vessels takes longer than in capillaries where RBCs rub along the capillary wall; decreasing PS_{cap} can give a good approximation to this enlarged resistance when the resistance and fluxes are calculated from a more detailed model such as that of Huang and Hellums.[44] Their model tested very well against the data on 1.5 mm diameter tubes from Dorson and Voorhees[28] on O_2 and CO_2 exchange. Fortunately the fluxes across walls of arterioles and venules are small,[44,67] so finding an exact correction is not critical. As for intra-tissue diffusion, with half-intercapillary distances of about 8 microns in the heart,[6] the diffusion relaxation times are short enough ($\tau = R^2/2D$ or about 30 ms maximum) that the radial gradients are almost dissipated within one time step for the numerical solution, allowing us to consider them negligible within the shorter distances across each of the radial regions.

Issue 3 relates to the hematocrit-dependency of the effective blood–tissue exchange, defined by Hellums[36] in a nicely principled analysis: Transfer of O_2 is faster when plasmatic gaps between RBC are smaller. Others[29,30,34,37,44] discussed that even in steady-state modeling there was an influence of RBC spacing in the capillary on the efficiency of O_2 transfer from blood to the tissue when the hematocrit was lower than 20%. This is not directly addressed in the current model, but the reduction in oxygen transfer due to the decreased P_{O_2} within the plasmatic gaps can be well

approximated, as far as delivery to the tissue is concerned, by an appropriate reduction in PS_{cap}.

Slow release of O_2 from Hb (Issue 4) retards exchange into peripheral tissues. Slow dissociation reduces the effective free O_2 concentration at the RBC membrane and reduces transmembrane flux,[37] exactly analogous to the situation for albumin-facilitated diffusion of fatty acid in plasma when there is endothelial uptake.[4] Likewise, slow association retards RBC uptake of O_2 in the lung, contributing to any alveolar–arterial O_2 concentration difference. Knowing the rate constants and the dimensions involved allows translation into an equivalent increase in the membrane resistance. While the rate constants for CO_2 binding with Hb are known, those for O_2 binding are concentration-dependent and treated empirically, as described by Hellums *et al.*[37], their Eq. (7), where the "on" and "off" rates are defined as a function of HbO_2 saturation to account for the cooperativity.

Slow anion exchange (Issue 5) may be important at the RBC membrane because a delay in HCO_3^- and Cl^- exchange influences the pH inside the RBC. This would slow the pH change along the length of the exchange region, retarding the rise of pH and carbamino formation in the capillary blood (Fig. 2) and slowing CO_2 loss in the lung. This is not accounted for in our present model.

Finally, Issue 6: There is the release of about 0.7 mole H^+ per mole of O_2 binding to Hb, and 1.5–2 moles H^+ per mole of CO_2 binding to Hb,[42] that are not included in the present model, but could be added stoichiometrically to the equation for H^+ fluxes. In going from a P_{O_2} of 40–100 mmHg, 1 mole of Hb goes from 75 to 98% saturated, a gain of 23%. With [Hb] = 7.2 mM (Table 1), the O_2 binding would displace about 0.7 times 0.23 times 7.2 mM, a change in $[H^+]$ of 1.16 mM, over 3 pH units. Since CO_2 binds less readily to HbO_2 than to Hb, and since in the lung the CO_2 is coming off when O_2 is going on, and vice versa in the systemic tissue, the net H^+ exchange is always smaller than 1.16 mM. Because the amount of CO_2 bound to Hb is much less than O_2, there is still a net H^+ balance dominated by the O_2 binding or release.

While it is important to address the preceding six issues in any model of O_2 and CO_2 exchange, the present model is comprehensive enough that the model parameters can be varied to fit many different physiological and pathological conditions. For example, one can look at the distributions of O_2, CO_2, HCO_3^-, and H^+ and the regulation of acid–base balance in tissue cells in normoxia, hypoxic hypoxia (low arterial P_{O_2}), and anemic hypoxia (low hematocrits) conditions, and with varying arterial plasma or RBC pH. The results shown in this paper (Figs. 3–6) are the simulated concentration profiles with decreasing blood flow (F_{bl}) and increasing O_2 consumption (V_{max}). These cases correspond to the ischemic or low-perfusion (low F_{bl}) and exercise or higher energy demand (high V_{max}) conditions. The transient behavior of these profiles at the onset of exercise (step increase in V_{max}) from steady state can be computed and analyzed in understanding the dynamics of O_2–CO_2 exchange and acid–base balance.

The respiratory quotient RQ (the ratio of CO_2 production to O_2 consumption) was fixed at an average value of 0.8 (protein metabolism). While RQ can vary from 0.7 (fat metabolism) to 1.0 (carbohydrate metabolism), a model for a regulated change in CO_2 production would require the model to include the major metabolic pathways (glycolysis, glycogenolysis, and TCA cycle) and oxidative phosphorylation[15,49] along with the present model to complete the link between O_2 consumption and CO_2 and H^+ production in the parenchymal cells.

There are 16 axial dispersion coefficients (^sD_r; 4 species × 4 regions) and 12 permeability surface area products (^sPS_m; 4 species × 3 membranes) in the current model. There is neither enough information nor a real necessity to set them all at distinct values, because the gas exchanges between regions are so rapid. As discussed above and in the "Mathematical Formulation of the Model" section, the Ds were assigned higher values than the pure molecular diffusion coefficients to account for the heterogeneities of spacing and capillary entrance regions. The radial diffusion is a separate issue. While the true membrane PSs are high, and must be for O_2 whose exchange is almost flow-limited in the microcirculation,[51] they are reduced somewhat to account for the retarding influences of diffusion as discussed above. The PSs for O_2 and CO_2 are set at the values used for O_2 by Li *et al.*[51] in their studies of PET data analysis. The PSs for HCO_3^- and H^+ are set one order of magnitude lower than those for O_2 and CO_2, because their molecular polarity reduces transmembrane transport compared to nonpolar solutes.

In conclusion, the present model describes physiologically realistic features of O_2 transport, exchange, and metabolism, including the simultaneous CO_2 transport and exchange and acid–base balance. It is rather general and is widely applicable to measuring O_2 consumption in the heart and other organs. The model parameters can be varied to simulate different physiological situations. The model is computationally efficient, so the tracer transients can be computed quickly, favoring this model as a preferred vehicle for routine data analysis (e.g., in PET imaging studies).

APPENDIX: ERRATA IN THE 2004 PUBLICATION OF THE HbO_2 AND $HbCo_2$ DISSOCIATION CURVES

Dash and Bassingthwaighte (2004): The article by Dash and Bassingthwaighte (Ann Biomed Eng **32**: 1676–1693, 2004) appeared in print without galley proofs having been sent to either of the authors for review and correction. Errors in print setting were such that the equations essential to reproducing the scientific work need to be reprinted in order

to make the present paper understandable and the original work reproducible. This appendix corrects the errors in the 2004 printing by providing the original, correct equations and text.

Correction 1: On page 1678 under MATHEMATICAL FORMULATIONS, Beginning at the end of paragraph 1, are a series of corrections to the equations 2a–f, where an upper case K is to be used instead of an erroneous lower case k:

"The governing reactions are:

CO_2 hydration reaction – HCO_3^- buffering of CO_2:

$$CO_2 + H_2O \underset{kb_1'}{\overset{kf_1'}{\rightleftarrows}} H_2CO_3 \overset{K_1''}{\rightleftarrows} HCO_3^- + H^+. \tag{2a}$$

CO_2 binding to $HmNH_2$ chains – $HmNHCOO^-$ buffering of CO_2:

$$CO_2 + HmNH_2 \underset{kb_2'}{\overset{kf_2'}{\rightleftarrows}} HmNHCOOH \overset{K_2''}{\rightleftarrows} HmNHCOO^- + H^+. \tag{2b}$$

CO_2 binding to O_2HmNH_2 chains – $O_2HmNHCOO^-$ buffering of CO_2:

$$CO_2 + O_2HmNH_2 \underset{kb_3'}{\overset{kf_3'}{\rightleftarrows}} O_2HmNHCOOH \overset{K_3''}{\rightleftarrows} O_2HmNHCOO^- + H^+. \tag{2c}$$

O_2 binding to $HmNH_2$ chains – one-step kinetics using the P_{O_2}-dependent values of the rates of association and dissociation to accounts for the cooperativity.

$$O_2 + HmNH_2 \underset{kb_4'}{\overset{kf_4'}{\rightleftarrows}} O_2HmNH_2. \tag{2d}$$

Ionization of $HmNH_2$ chains – pH buffering:

$$HmNH_3^+ \overset{K_5''}{\rightleftarrows} HmNH_2 + H^+. \tag{2e}$$

Ionization of O_2HmNH_2 chains – pH buffering:

$$O_2HmNH_3^+ \overset{K_6''}{\rightleftarrows} O_2HmNH_2 + H^+. \tag{2f}$$

Correction 2: On page 1679, in the last sentence of this same section, and ending just above the section heading "*Equilibrium Relations*" the "k_4'" should be replaced by the upper case K_4' in two places:

"To account for this through our one-step kinetic approach in reaction (2d), we use the equilibrium "constant" $K_4'(= kf_4'/kb_4')$ a function of O_2 partial pressure P_{O_2}; K_4' also depends on the levels of pH, P_{CO_2}, 2,3-DPG concentration, and temperature inside the RBCs[4]."

Correction 3: All of Equations 3 and 4 require corrections to the upper versus lower case Ks and the kfs in the section on Equilibrium Relations:

$$K_1'\,[CO_2] = [H_2CO_3], \tag{3a}$$

$$K_1''\,[H_2CO_2] = [HCO_3^-][H^+], \tag{3b}$$

$$K_2'\,[CO_2][HmNH_2] = [HmNHCOOH], \tag{3c}$$

$$K_2''\,[HmNHCOOH] = [HmNHCOO^-][H^+], \tag{3d}$$

$$K_3'\,[CO_2][O_2HmNH_2] = [O_2HmNHCOOH], \tag{3e}$$

$$K_3''\,[O_2HmNHCOOH] = [O_2HmNHCOO^-][H^+], \tag{3f}$$

$$K_4'\,[O_2][HmNH_2] = [O_2HmNH_2], \tag{3g}$$

$$K_5''\,[HmNH_3^+] = [HmNH_2][H^+], \tag{3h}$$

$$K_6''\,[O_2HmNH_3^+] = [O_2HmNH_2][H^+], \tag{3i}$$

where the equilibrium constants K_1', K_2', K_3' and K_4' are defined by

$$K_1' = \frac{kf_1'}{kb_1'}[H_2O], \quad K_2' = \frac{kf_2'}{kb_2'}, \quad K_3' = \frac{kf_3'}{kb_3'}, \quad K_4' = \frac{kf_4'}{kb_4'}. \tag{4}$$

Correction 4: In Appendix A, Eq. A.2 should be corrected to read:

$$[CO_2]_{bl} = W_{bl}\alpha_{CO_2}P_{CO_2} + [HCO_3^-]_{bl} + 4[Hb]_{bl}S_{HbCO_2}, \tag{A.2}$$

Correction 5: The last sentence in the paragraph below Eq. A.3 should correct R_{rbc} to read:

"The value of R_{rbc} is about 0.69[13–15,31,38]. Multiplying $[CO_2]_{bl}$ by 22.256 converts the units of molar to ml of CO_2 per ml of blood."

Correction 6: The first sentence of the paragraph above Eq. A.4 should correct H_2O:

"From the data used in Hill et al.[13–15], $[H_2O]\ kf_1' \approx 0.12\ s^{-1}$ and $kb_1' \approx 89\ s^{-1}$, so $K_1' = [H_2O]\ kf_1'/kb_1' \approx 1.35 \times 10^{-3}$."

Correction 7: In Appendix B, Eqs. B.1 to B.3 should be corrected re K'_{HbO_2} and K_{fact} and the latter part of the first paragraph corrected to read:

"

$$S_{HbO_2} = \frac{K'_{HbO_2}[O_2]^{1+n_0}}{1 + K'_{HbO_2}[O_2]^{1+n_0}}, \tag{B.1}$$

where K'_{HbO_2} (with units $M^{-(1+n_0)}$) is given by Equations 13 and 14:

$$K'_{HbO_2} = \frac{K''_4 K_{fact}}{K_{ratio}[O_2]_S^{n_0}} = \frac{1}{(\alpha_{O_2} P_{50})^{1+n_0}}, \qquad (B.2)$$

The P_{50} is defined as before by Eq. (11) and the kinetic terms K_{ratio} and K_{fact} are defined by Eqs. (18) and (14b). The Hill exponent in the expression for S_{HbO_2} is now $1 + n_0$ and apparent Hill coefficient K'_{HbO_2} is now independent of $[O_2]$. This makes S_{HbO_2} analytically invertible, when P_{CO_2}, pH, [DPG] and T are known. The inverted equation for $[O_2]$ is given by

$$[O_2] = \left[\frac{S_{HbO_2}}{K'_{HbO_2}(1 - S_{HbO_2})}\right]^{\frac{1}{1+n_0}} = \alpha_{O_2} P_{50} \left[\frac{S_{HbO_2}}{1 - S_{HbO_2}}\right]^{\frac{1}{1+n_0}}. \qquad (B.3)$$

It is clear from Eq. (2) that K'_{HbO_2} can be determined completely using only the $P_{50} = P_{50}([H^+], [CO_2], [DPG], T)$ data which is given by Eq. (11). This avoids the calculations of K_{ratio} and K_{fact} which involves the complex computations of the empirical indices n_1, n_2, n_3, and n_4 using Eqs. (20a) to (20d). This also simplifies the computation of S_{HbO_2} from $[O_2]$ and vice-versa significantly. However, in the computation of S_{HbCO_2} from $[CO_2]$ and vice-versa (not shown in this appendix), the calculations of K_{fact} and K_{ratio} are essential as the P_{50} data for 50% $HbCO_2$ saturation is not available in the literature."

ACKNOWLEDGMENTS

This research was supported by the National Simulation Resource Facility for Circulatory Mass Transport and Exchange via the grants P41-RR1243 from NCRR/NIH and R01-EB001973 from NIBIB/NIH. RKD was partially supported by the Center for Modeling Integrated Metabolic Systems (MIMS) via grant P50-GM66309 from NIGMS/NIH. The authors are grateful to the reviewers for their useful comments and suggestions. The model code is available at http://nsr.bioeng.washington.edu/ and can be run there via an applet supported by NIH/NIBIB R01-EB001973.

REFERENCES

[1] Antonini, E., and M. Brunori. Hemoglobin and Myoglobin in their Reactions with Ligands. Amsterdam: North Holland, 1971, 436 pp.

[2] Austin, W. H., E. Lacombe, P. W. Rand, and M. Chatterjee. Solubility of carbon dioxide in serum from 15 to 38°C. *J. Appl. Physiol.* 18:301–304, 1963.

[3] Barbee, J. H., and G. R. Cokelet. The Fahraeus effect. *Microvasc. Res.* 3:6–16, 1971.

[4] Barta, E., S. Sideman, and J. B. Bassingthwaighte. Facilitated diffusion and membrane permeation of fatty acid in albumin solutions. *Ann. Biomed. Eng.* 28:331–345, 2000.

[5] Bassingthwaighte, J. B. Plasma indicator dispersion in arteries of the human leg. *Circ. Res.* 19:332–346, 1966.

[6] Bassingthwaighte, J. B., T. Yipintsoi, and R. B. Harvey. Microvasculature of the dog left ventricular myocardium. *Microvasc. Res.* 7:229–249, 1974.

[7] Bassingthwaighte, J. B. A concurrent flow model for extraction during transcapillary passage. *Circ. Res.* 35:483–503, 1974.

[8] Bassingthwaighte, J. B., T. Yipintsoi, and T. J. Knopp. Diffusional arteriovenous shunting in the heart. *Microvasc. Res.* 28:233–253, 1984.

[9] Bassingthwaighte, J. B., and C. A. Goresky. Modeling in the analysis of solute and water exchange in the microvasculature. In: Handbook of Physiology. Sect. 2, The Cardiovascular System. Vol IV, The Microcirculation, edited by E. M. Renkin and C. C. Michel. Bethesda, MD: *Am. Physiol. Soc.*, 1984, pp. 549–626.

[10] Bassingthwaighte, J. B., F. P. Chinard, C. Crone, C. A. Goresky, N. A. Lassen, R. S. Reneman, and K. L. Zierler. Terminology for mass transport and exchange. *Am. J. Physiol. Heart Circ. Physiol.* 250:H539–H545, 1986.

[11] Bassingthwaighte, J. B., C. Y. Wang, and I. S. Chan. Blood–tissue exchange via transport and transformation by endothelial cells. *Circ. Res.* 65:997–1020, 1989.

[12] Bassingthwaighte, J. B., R. B. King, and S. A. Roger. Fractal nature of regional myocardial blood flow heterogeneity. *Circ. Res.* 65:578–590, 1989.

[13] Bassingthwaighte, J. B., I. S. Chan, and C. Y. Wang. Computationally efficient algorithms for capillary convection-permeation-diffusion models for blood–tissue exchange. *Ann. Biomed Eng.* 20:687–725, 1992.

[14] Bassingthwaighte, J. B., D. A. Beard, and Z. Li. The mechanical and metabolic basis of myocardial blood flow heterogeneity. *Basic Res. Cardiol.* 96:582–594, 2001.

[15] Bassingthwaighte, J. B. The modelling of a primitive "sustainable" conservative cell. *Philos. Trans. R. Soc. Lond. A* 359:1055–1072, 2001.

[16] Beard, D. A., and J. B. Bassingthwaighte. Advection and diffusion of substances in biological tissues with complex vascular networks. *Ann. Biomed. Eng.* 28:253–268, 2000.

[17] Beard, D. A., and J. B. Bassingthwaighte. Modeling advection and diffusion of oxygen in complex vascular networks. *Ann. Biomed. Eng.* 29:298–310, 2001.

[18] Beard, D. A. Computational framework for generating transport models from databases of microvascular anatomy. *Ann. Biomed. Eng.* 29:837–843, 2001.

[19] Berzins, M., and P. M. Dew. Algorithm 690: Chebyshev polynomial software for elliptic-parabolic systems of PDEs. *ACM Trans. Math. Softw.* 17:178–206, 1994.

[20] Beyer, R. P., J. B. Bassingthwaighte, and A. J. Deussen. A computational model of oxygen transport from red blood cells to mitochondria. *Comput. Methods. Prog. Biomed.* 67:39–54,2002.

[21] Blom, J. G., and P. A. Zegeling. Algorithm 731: A moving grid-interface for systems of one-dimensional time-dependent partial differential equations. *ACM Trans. Math. Softw.* 20:194–214, 1994.

[22] Buerk, D. G., and E. W. Bridges. A simplified algorithm for computing the variation in oxyhemoglobin saturation with pH P_{CO_2}, T and DPG. *Chem. Eng. Commun.* 47:113–124, 1986.

[23] Butterworth, E., and Z. Li. JSim, a Java-based simulation system for modeling analysis of experimental data. http://nsr.bioeng.washington.edu/, Seattle, Washington:2000.

[24] Caldwell, J. H., G. V. Martin, G. M. Raymond, and J. B. Bassingthwaighte. Regional myocardial flow and capillary permeability–surface area products are nearly proportional. *Am. J. Physiol. Heart Circ. Physiol.* 267:H654–H666, 1994.

[25]Colombo, M. F., D. C. Rau, and V. A. Parsegian. Protein solvation in allosteric regulation: A water effect on hemoglobin. *Science* 256:655–659, 1992.

[26]Dash, R. K., and J. B. Bassingthwaighte. Blood HbO_2 and $HbCO_2$ dissociation curves at varied O_2, CO_2, pH, 2,3-DPG and temperature levels. *Ann. Biomed. Eng.* 32:1676–1693, 2004.

[27]Deussen, A., and J. B. Bassingthwaighte. Modeling [^{15}O]oxygen tracer data for estimating oxygen consumption. *Am. J. Physiol. Heart Circ. Physiol.* 270:H1115–H1130,1996.

[28]Dorson, W. J., Jr., and M. Voorhees. Limiting models for the transfer of CO_2 and O_2 in membrane oxygenators. *Trans. Am. Soc. Artif. Intern. Organs* 20A:219–226, 1974.

[29]Federspiel, W. J., and I. H. Sarelius. An examination of the contribution of red cell spacing to the uniformity of oxygen flux at the capillary wall. *Microvasc. Res.* 27:273–285, 1984.

[30]Federspiel, W. J., and A. S. Popel. A theoretical analysis of the effect of the particulate nature of blood on oxygen release in capillaries. *Microvasc. Res.* 32:164–189, 1986.

[31]Goldman, D., and A. S. Popel. A computational study of the effect of capillary network anastomoses and tortuosity on oxygen transport. *J. Theor. Biol.* 206:181–194, 2000.

[32]Gonzalez, F., and J. B. Bassingthwaighte. Heterogeneities in regional volumes of distribution and flows in the rabbit heart. *Am. J. Physiol. Heart Circ. Physiol.* 258:H1012–H1024, 1990.

[33]Goresky, C. A., G. G. Bach, and B. E. Nadeau. Red cell carriage of label: Its limiting effect on the exchange of materials in the liver. *Circ. Res.* 36:328–351, 1975.

[34]Groebe, K., and G. Thews. Effects of red cell spacing and red cell movement upon oxygen release under conditions of maximally working skeletal muscle. In: Oxygen Transport to Tissue XI, edited by K. Rakusan, G. P. Biro, T. K. Goldstick, and Z. Turek. New York: Plenum Press, 1989, pp. 175–185.

[35]Hedley-Whyte, J., and M. B. Laver. O_2 solubility in blood and temperature correction factors for PO_2. *J. Appl. Physiol.* 19:901–906, 1964.

[36]Hellums, J. D. The resistance to oxygen transport in the capillaries relative to that in the surrounding tissue. *Microvasc. Res.* 13:131–136, 1977.

[37]Hellums, J. D., P. K. Nair, N. S. Huang, and N. Ohshima. Simulation of intraluminal gas transport processes in the microcirculation. *Ann. Biomed. Eng.* 24:1–24, 1996.

[38]Hill, A. V. The possible effects of the aggregation of the molecules of haemoglobin on its dissociation curves. *J. Physiol.* 40:iv–vii, 1910.

[39]Hill, E. P., G. G. Power, and L. D. Longo. A mathematical model of carbon dioxide transfer in the placenta and its interaction with oxygen. *Am. J. Physiol. Cell Physiol.* 224:283–299, 1973.

[40]Hill, E. P., G. G. Power, and L. D. Longo. Mathematical simulation of pulmonary O_2 and CO_2 exchange. *Am. J. Physiol. Cell Physiol.* 224:904–917, 1973.

[41]Hill, E. P., G. G. Power, and L. D. Longo. Kinetics of O_2 and CO_2 exchange. In: Bioengineering Aspects of the Lung, edited by J. B. West. New York: Marcel Dekker, 1977, pp. 459–514.

[42]Hlastala, M. P., and R. D. Woodson. Saturation dependency of the Bohr effect: Interactions among H^+, CO_2 and DPG. *J. Appl. Physiol.* 38:1126–1131, 1975.

[43]House, S. D., and H. H. Lipowsky. Microvascular hematocrit and red cell flux in rat cremaster muscle. *Am. J. Physiol. Heart Circ. Physiol.* 252:H211–H222, 1987.

[44]Huang, N. S., and J. D. Hellums. A theoretical model for gas transport and acid/base regulation by blood flowing in microvessels. *Microvasc. Res.* 48:364–388, 1994.

[45]Kelman, G. R. Digital computer subroutine for the conversion of oxygen tension into saturation. *J. Appl. Physiol.* 21:1375–1376, 1966.

[46]Kettunen, M. I., O. H. J. Gröhn, M. J. Silvennoinen, M. Penttonen, and R. A. Kauppinen. Quantitative assesment of balance between oxygen delivery and consumption in the rat brain after transient ischemia with T_2-BOLD magnetic resonance imaging. *J. Cereb. Blood Flow Metab.* 22:262–270, 2002.

[47]King, R. B., J. B. Bassingthwaighte, J. R. S. Hales, and L. B. Rowell. Stability of heterogeneity of myocardial blood flow in normal awake baboons. *Circ. Res.* 57:285–295, 1985.

[48]King, R. B., G. M. Raymond, and J. B. Bassingthwaighte. Modeling blood flow heterogeneity. *Ann. Biomed. Eng.* 24:352–372,1996.

[49]Korzeniewski, B., and J. A. Zoladz. A model of oxidative phosphorylation in mammalian skeletal muscle. *Biophys. Chem.* 92:17–34, 2001.

[50]Krogh, A. The number and distribution of capillaries in muscles with calculations of the oxygen pressure head necessary for supplying the tissue. *J. Physiol. (Lond.)* 52:409–415, 1919.

[51]Li, Z., T. Yipintsoi, and J. B. Bassingthwaighte. Nonlinear model for capillary–tissue oxygen transport and metabolism. *Ann. Biomed. Eng.* 25:604–619, 1997.

[52]Nair, P. K., D. G. Buerk, and W. J. Whalen. Cat carotid body oxygen metabolism and chemoreception described by a two-cytochrome model. *Am. J. Physiol. Heart Circ. Physiol.* 250:H202–H207, 1986.

[53]Ogawa, S., R. S. Menon, D. W. Tank, S. G. Kim, H. Merkle, J. M. Ellermann, and K. Ugurbil. Functional brain mapping by blood oxygenation level-dependent contrast magnetic resonance imaging. A comparison of signal characteristics with a biophysical model. *Biophys. J.* 64:803–812, 1993.

[54]Popel, A. S. Theory of oxygen transport to tissue. *Crit. Rev. Biomed. Eng.* 17:257–321, 1989.

[55]Rose, C. P., and C. A. Goresky. Limitations of tracer oxygen uptake in the canine coronary circulation. *Circ. Res.* 56:57–71, 1985.

[56]Safford, R. E., and J. B. Bassingthwaighte. Calcium diffusion in transient and steady states in muscle. *Biophys. J.* 20:113–136, 1977.

[57]Safford, R. E., E. A. Bassingthwaighte, and J. B. Bassingthwaighte. Diffusion of water in cat ventricular myocardium. *J. Gen. Physiol.* 72:513–538, 1978.

[58]Salathe, E. P., R. Fayad, and S. W. Schaffer. Mathematical analysis of carbon dioxide transfer by blood. *Math. Biosci.* 57:109–153, 1981.

[59]Schenkman, K. A., D. R. Marble, D. H. Burns, and E. O. Feigl. Myoglobin oxygen dissociation by multiwavelength spectroscopy. *J. Appl. Physiol.* 82:86–92, 1997.

[60]Schenkman, K. A., D. R. Marble, D. H. Burns, and E. O. Feigl. Optical spectroscopic method for *in vivo* measurement of cardiac myoglobin oxygen saturation. *Appl. Spectrosc.* 53:332–338, 1999.

[61]Secomb, T. W., R. Hsu, N. B. Beamer, and B. M. Coull. Theoretical simulation of oxygen transport to brain by networks of microvessels: Effects of oxygen supply and demand on tissue hypoxia. *Microcirculation* 7:237–247, 2000.

[62]Shishido, F., K. Uemura, A. Inugami, T. Ogawa, T. Yamaguchi, I. Kanno, M. Murakami, K. Tagawa, and N. Yasui. Remote effects in MCA territory ischemic infarction: A study of regional cerebral blood flow and oxygen metabolism using positron computed tomography and ^{15}O labeled gases. *Radiat. Med.* 5:36–41, 1987.

[63]Singh, M. P., M. Sharan, and A. Aminataei. Development of mathematical formulae for O_2 and CO_2 dissociation curves in the blood. *IMA J. Math. Appl. Med. Biol.* 6:25–46, 1989.

[64]Suenson, M., D. R. Richmond, and J. B. Bassingthwaighte. Diffusion of sucrose, sodium, and water in ventricular myocardium. *Am. J. Physiol.* 227:1116–1123, 1974.

[65] Vinnakota, K., and J. B. Bassingthwaighte. Myocardial density and composition: A basis for calculating intracellular metabolite concentrations. *Am. J. Physiol. Heart Circ. Physiol.* 286:H1742–H1749, 2004.

[66] Winslow, R. M., M. Samaja, N. J. Winslow, L. Rossi-Bernardi, and R. I. Shrager. Simulation of continuous blood O_2 equilibrium over physiological pH, DPG, and PCO_2 range. *J. Appl. Physiol.: Respir. Environ. Exercise Physiol.* 54:524–529, 1983.

[67] Ye, G. F., T. W. Moore, D. G. Buerk, and D. Jaron. A compartmental model for oxygen-carbon dioxide coupled transport in the microcirculation. *Ann. Biomed. Eng.* 22:464–479, 1994.